

Geology of the Darreh-Zerreshk and Ali-Abad Porphyry Copper Deposits, Central Iran

A. ZARASVANDI, S. LIAGHAT,

Department of Earth Sciences, Shiraz University, P.O. Box 1330, Shiraz, Iran

AND M. ZENTILLI¹

Department of Earth Sciences, Dalhousie University, Halifax, Nova Scotia, Canada B3H 4J1

Abstract

This paper describes the petrology, mineralogy, alteration, structural characteristics, and geological evolution of the Darreh-Zerreshk and Ali-Abad copper deposits within the central Iranian volcano-plutonic belt, Yazd Province, central Iran. Intrusions in this area, a result of subduction magmatism, range in composition from quartzmonzodiorite to granite, yet copper-molybdenum porphyry-type mineralization is restricted to quartzmonzodioritic to granodioritic plutons. The mineralizing intrusions cut Cretaceous and Eocene strata, and have been dated as Oligocene–Miocene. Strong negative anomalies for Nb, Ta, P, and Ti and enrichment in the LREE, LILE, Ba, Rb, Sr, and Pb for the mineralizing igneous rocks suggest they are of I type and have magmatic arc affinity. REE patterns, major-, and trace-element data suggest that these rocks were derived from partial melting of enriched upper mantle, modified by variable crustal contamination. Hornblende fractionation was an important control on the evolution of copper-bearing plutonic rocks. Structural observations suggest that these deposits were emplaced in tensional pull-apart domains formed between two secondary dextral strike-slip faults of the regional Dehshir-Baft shear system. Rapid exhumation of the porphyry copper systems allowed for the development of only minor supergene enrichment.

Introduction

ALL KNOWN PORPHYRY-type copper deposits in Iran are associated with Neogene granitoids within the central Iranian volcano-plutonic belt (CIVPB), also known as the Urumieh-Dokhtar belt (e.g., Bazin and Hubner, 1969; Jankovic, 1984). This plutonic-metallogenic belt parallels the Zagros fold-and-thrust belt, northeast of the main thrust fault zone, and an intervening longitudinal tectonic depression (Fig. 1). Volcanism, plutonism, and associated mineralization in the CIVPB are considered to be the result of subduction (e.g., Berberian and King, 1981) within the collisional Zagros belt.

The largest known porphyry copper deposits of Iran, Sungun and Sar-Cheshmeh, which are currently mined, are located in the northwestern and southeastern sections of the CIVPB, respectively (Fig. 1). The Sungun porphyry stocks are Oligocene–Miocene in age and intruded Cretaceous carbonate and Eocene volcano-sedimentary rocks (Hezarkhani and Williams-Jones, 1998). Sungun

contains more than 500 Mt of hypogene sulfide ore at 0.75% Cu and 0.01% Mo (unpublished data, National Iranian Copper Industries Co., or NICICO). The Miocene Sar-Cheshmeh porphyry intruded Eocene andesites and contains 1,200 Mt of sulfide ore at an average grade of 1.2% Cu, 0.03% Mo, 0.27 g/t Au, and 3.9 g/t Ag (Ellis, 1991).

Exploration carried out by the Geological Survey of Iran (GSI), and Yugoslavian, Australian, Canadian, and French mining companies between 1966 and 2003 have identified many copper deposits and occurrences along the CIVPB. Two of these, the Darreh-Zerreshk and Ali-Abad copper deposits, the subject of this paper, have recently been reassessed during national reconnaissance programs carried out by NICICO. There have been no previous detailed geological, structural, petrogenetic, and geochronological studies on the Darreh-Zerreshk and Ali-Abad deposits.

Darreh-Zerreshk (UTM 769000N/3495000E) and Ali-Abad (UTM 769000N/ 3504800 E) are located ~60 km southwest of the city of Yazd in central Iran at an elevation of 2,600 to 3,000 m above sea level (Figs. 1 and 2). The access road is the main

¹Corresponding author; email: zentilli@dal.ca

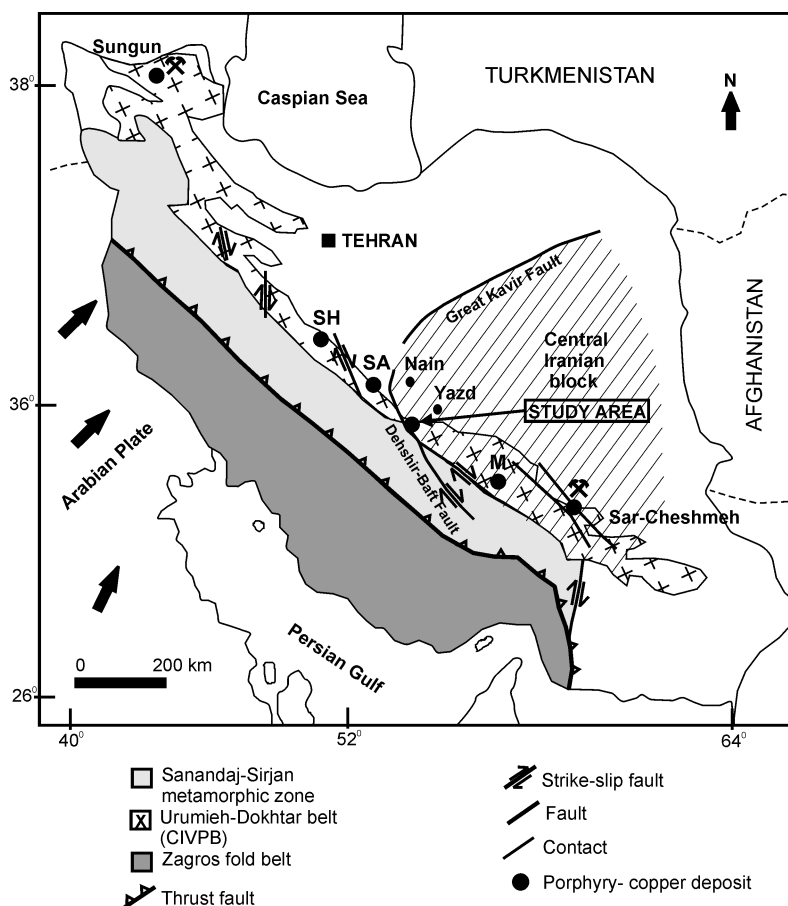


FIG. 1. Index map showing the geographical position and main tectonic zones of Iran. Dashed area is the central Iranian block. Abbreviations: M = Meiduk porphyry copper deposit; SA = southern portion of Ardestan porphyry copper deposit; SH = Sharifabad porphyry copper deposit. Black arrows indicate relative plate motion from Sokoutis et al. (2000).

paved highway from Shiraz city to Yazd. Both deposits were revealed in 1972 as a result of geophysical surveys and drilling by the French company COFIMINS. Drillhole data and surface outcrops were used to produce the first geological reports, which recognized these deposits as porphyry type mineralization (COFIMINS, 1972; NICICO, 2001). Assessment drilling defined indicated resources of 40 Mt at 0.73% Cu, 0.0059% Mo, and 19 g/t Ag for the Ali-Abad deposit (NICICO, 2001), and 23 Mt at 0.8 to 0.97% Cu, 0.0040% Mo, and 1 g/t Ag for Darreh-Zerreshk (COFIMINS, 1972).

Copper ore minerals in the Ali-Abad and Darreh-Zerreshk deposits consist of three main

assemblages: hypogene sulfides, supergene sulfides, and copper oxides. The total resource at Darreh-Zerreshk is 8.9 Mt of oxide ore at 0.8% Cu and 14.6 Mt of sulfide at 0.95% Cu. In Ali-Abad, a total resource consists of sulfide ore at 0.9 % Cu average grade (NICICO, 2001).

In this paper we present the results of new geological mapping, geochemical analyses carried out to better characterize and to study igneous petrogenesis of the mineralizing ore-bearing rocks, and a structural study aimed at establishing the structural controls of the Darreh-Zerreshk and Ali-Abad deposits. Detailed geochronology is presented elsewhere (Zarasvandi et al., 2004).

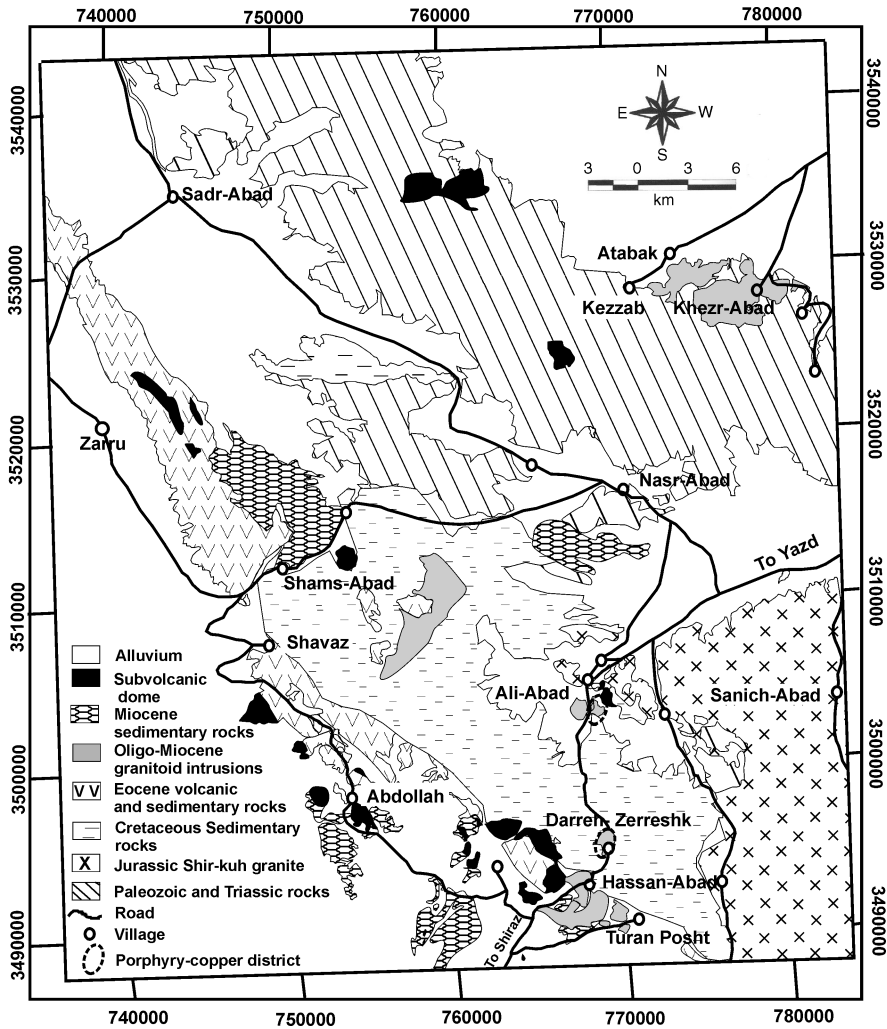


FIG. 2. Simplified regional geological map of southwestern Yazd Province (central Iran), modified from the Khezar-Abad geology map 1:100,000, Geological Survey of Iran.

Regional Geologic Setting

The geotectonic setting of Iran with respect to the Scytho-Turanian plate in the north and the Arabian plate (Gondwana) in the south is still a matter of controversy (e.g. Soffel et al., 1996). Subduction between the Iranian and Afro-Arabian plates during the Mesozoic defined three main parallel tectonic zones: (1) the Zagros fold-and-thrust belt; (2) the Sanandaj-Sirjan metamorphic zone; and (3) the CIVPB (Fig. 1). Most Iranian igneous rocks associated with Cu mineralization are in the CIVPB. This

magmatic belt is considered to be an integral part of the Zagros orogenic belt (e.g., Stocklin, 1968; Alavi, 1994), which in turn is part of the Alpine-Himalayan orogenic/metallogenic belt, and extends from the Eastern Anatolian fault in eastern Turkey to the Oman line in southern Iran, a distance of over 2000 km. Early studies suggested either a subduction model (e.g., Takin, 1972; Forster, 1978; Niazi and Asoudeh, 1978; Alavi, 1980; Berberian, et al., 1982; Chevren, 1986) or a continental rifting model (e.g., Sabzehe, 1974; Amidi, 1975) for the tectonic setting and formation of the Zagros orogenic belt.

According to the subduction model, a small continental block (the Central Iranian block, CIRB) separated from Gondwana in the early Mesozoic and formed the Iranian plate and a Neo-Tethys basin, floored by oceanic crust (Alavi, 1980; Sengör, 1990). In the Early Cretaceous, movement of the Iranian plate and the Neo-Tethys oceanic crust ceased, resulting first in the subduction of the Neo-Tethyan oceanic lithosphere under the CIRB, and subsequently in the collision between the Afro-Arabian and Iranian plates. In contrast, the continental rifting model assumed that magmatism in the central Iranian block resulted from the episodic opening of a continental rift zone during the Eocene. Most recent work, however, fully supports the subduction model (e.g., Alavi, 1994), and also emphasizes the tectonic effects of oblique subduction (Sokoutis et al., 2000) in the generation of parallel strike-slip structures in the CIVPB.

CIVPB magmatic arc

Early studies of the central Iranian volcano-plutonic belt generally suggested that it represents an Andean type magmatic arc formed by subduction along the active continental margin of the central Iranian block during Alpine orogeny (Takin, 1972; Dewey et al., 1973; Berberian et al., 1982; Sengör, 1990; Alavi, 1994). However, other workers proposed that the belt was formed by post-collision magmatism related to orogenic collapse (e.g., Stocklin, 1974; Berberian and King, 1981). Late Mesozoic and Paleogene plutons intruded sedimentary rocks of Cretaceous age (Nabavi, 1976; Alavi, 1980). Magmatic activity in the CIVPB peaked during the Eocene, leading to widespread extrusion of volcanic rocks consisting of trachybasalt, andesite and dacite lavas, domes, ignimbrites, and tuffs (Alavi, 1980). These rocks were in turn intruded by granitoids of Oligocene–Miocene age, which in the central part of the CIVPB are spatially associated with copper mineralization (Jankovic, 1984).

Major structural features

With the closure of Neo-Tethys ocean, the Afro-Arabian tectonic plate started to be subducted beneath south-central Iran, developing a NE-dipping subduction zone; relative plate motions at an incidence angle of $\sim 45^\circ$ were responsible for oblique convergence and formation of collision-type subduction involving strike-slip shear (Alavi, 1980; Sokoutis et al., 2000; Mohajjel et al., 2003) from the Late Cretaceous to the Paleocene. Post-Paleocene

SW-vergent thrusting and strike-slip faulting with resulting shortening, shearing, and crustal thickening are consistent with a compressional regime. Extensive volcanic activity (Berberian and King, 1981) accompanied this compression. After the compressive stage, extensional faults and localized relaxation “rifting” developed in several parts of the Iranian continental margin. Calc-alkaline granitoid magmatism of the CIVPB is probably associated with this extensional episode (Berberian and King, 1981; Alavi, 1994).

Faults have played an important role in the emplacement of intrusions in the CIVPB and central Iranian block. The most important structures in the CIVPB are dextral strike-slip faults (Fig. 1). Many of these faults are associated with synkinematic magmatism as evidenced by the presence of granitoids and numerous dikes along zones adjacent and parallel or oblique to faults. Faults had an important role in controlling copper mineralization as well, (Shahabpour, 1996, 1999), and the analysis of lineaments from satellite images (e.g. Forster, 1978) led to the conclusion that porphyry copper deposits in the southeast section of CIVPB (central Iranian copper province) occur predominantly at the intersection of NNW-SSE and NW-SE faults with old deep structures. These structural relationships appear to be applicable to other areas of the CIVPB.

Methodology

Compilation of satellite images, maps and reports, and detailed geological mapping of the Darreh-Zerreshk and Ali-Abad areas were carried out by AZ and SL during the summers of 2000 and 2003. Representative samples of both unaltered and altered/mineralized rocks were collected for lithochemistry, described petrographically ($n = 50$), and analyzed for major elements ($n = 44$) and trace elements ($n = 20$). The thin sections of rocks were studied with a petrographic microscope at Shiraz University. Rock analyses were done by XRF and ICP-MS in the Kian Tief Zagros laboratory in Iran, and the Amdel Co. laboratory in Australia. Fracture analysis at the regional scale was done from satellite images, and available airborne geophysical survey maps. Field checks and systematic structural measurements were carried out in selected areas of both deposits, because it was recognized early that barren and mineralized fractures in these mineralized bodies have marked preferred orientations.

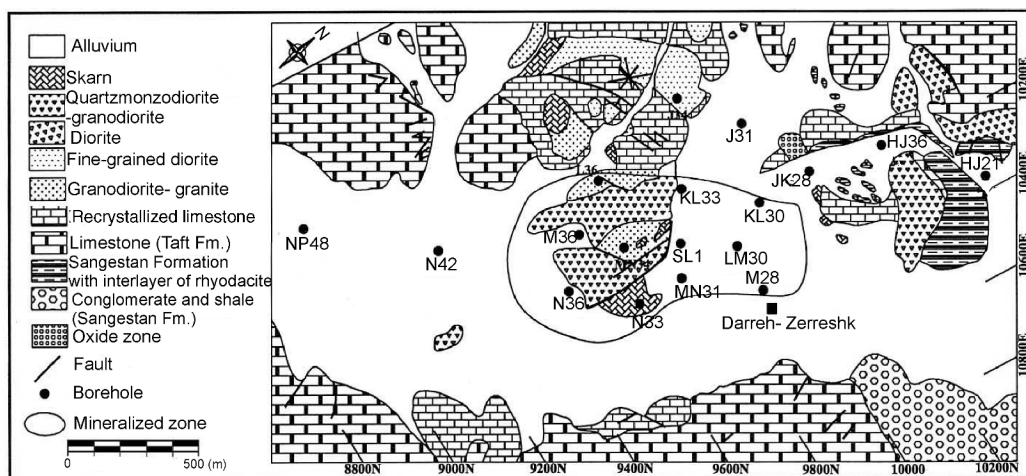


FIG. 3. Geological map of the Darreh-Zerreshk porphyry copper deposit (modified from COFIMINS, 1972).

Geology of the Darreh-Zerreshk and Ali-Abad Districts

The Darreh-Zerreshk and Ali-Abad deposits are located on the western boundary of the crustal central Iranian block, where it intersects the CIVPB (Fig. 1). The oldest units in the area (Fig. 2) are Paleozoic sedimentary rocks, and the Jurassic granitic Shir-Kuh batholith (Nabavi, 1972), which metamorphosed the host Paleozoic and Triassic units. The Shir-Kuh batholith is overlain unconformably by Lower Cretaceous conglomerates (Sangestan Formation; Nabavi, 1972; Khosrotehrani and Vazirimoghadam 1993). Upper Cretaceous conglomerate and sandstone units overlie unconformably the Lower Cretaceous strata; these clastic rocks grade upward to massive grey limestone of the Taft Formation (Nabavi, 1972; Khosrotehrani and Vazirimoghadam, 1993). The Mesozoic sedimentary sequence is in turn overlain by the Eocene conglomerate (Kerman Formation; Hajmolaali and Alavi Naeini, 1993) and volcanosedimentary rocks. Eocene volcanic activity consisted of andesitic lavas, trachyandesite, and pyroclastic rocks in the first stage, and two pulses that include dacitic domes and pyroclastic rocks in the late stage. Andesitic rocks with propylitic alteration occur in the western and southwestern parts of the study area (Fig. 2). Oligo-Miocene granitoid plutons (Zarasvandi et al., 2004) are in intrusive contact with Mesozoic and Paleocene units. These intrusive rocks in order of their relative intrusive age, consist of granite, granodiorite, quartzmonzodiorite,

tonalite, quartzdiorite, and diorite. They were emplaced in the northern (Ali-Abad intrusion), southern (Darreh-Zerreshk stocks), and southeastern (Touranposht intrusion) parts of the study area (Zarasvandi et al., 2002; Zarasvandi and Liaghat, 2003; Fig. 2). Neogene dacitic subvolcanic domes occur mainly in the southwestern section of the Darreh-Zerreshk area (Fig. 2); geothermal activity associated with these domes, which interacted with host limestone units, generated large deposits of green travertine.

Darreh-Zerreshk and Ali-Abad Porphyry Copper Deposits

Geology

In the western and eastern part of the Darreh-Zerreshk deposit, the sequence starts with Mesozoic strata (Fig. 3). These rocks are Upper Jurassic to Lower Cretaceous (Sangestan Formation) with conglomerate, sandstone, and red to dark grey shale (Nabavi, 1972). The Sangestan Formation was covered unconformably by layered to massive grey marine carbonates of the Barremian–Aptian Taft Formation. Eocene volcanosedimentary rocks (mostly rhyolitic tuffs) occur to the north and northeast of the Darreh-Zerreshk map area (Fig. 3), where the rocks were affected by argillic alteration. The Mesozoic–Paleocene sequence was intruded by granitic rocks (26 Ma K/Ar; Zarasvandi et al., 2004) and relatively more mafic granitoid complexes, ranging from fine-grained diorite (shown in the west-

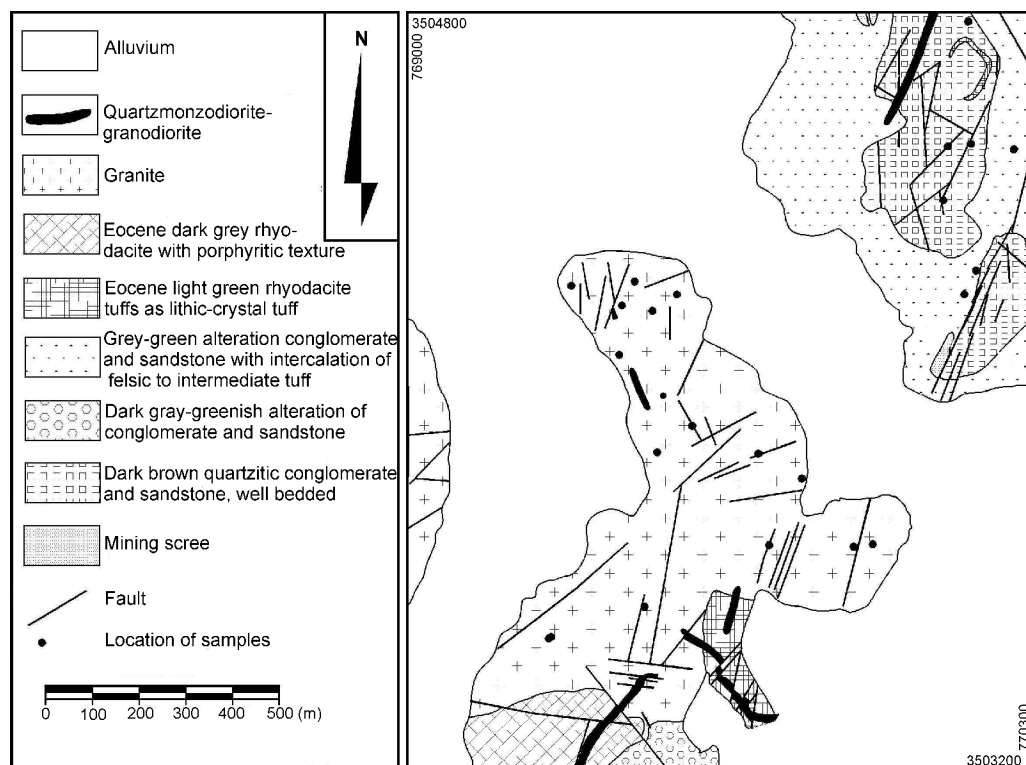


FIG. 4. Geological map of the Ali-Abad porphyry copper deposit. (modified from COFIMINS, 1972 and NICICO, 2001).

ern part of Fig. 3) and quartzdiorite–quartz monzodiorite (12–17 Ma K/Ar; Zarasvandi et al., 2004) in the exposed core of intrusion, shown as a mineralized zone in the map (Zarasvandi et al., 2004). Where unaltered, the intrusive rocks have porphyritic texture and hornblende and biotite as the main mafic phases. Near Cu mineralization in the Darreh-Zerreshk area, they show potassic alteration. Intrusion of these granitoid stocks into the carbonate rocks in the Darreh-Zerreshk has developed sub-economic skarn-type Fe-Cu mineralization (Fig. 3).

The oldest rocks cropping out at Ali-Abad are well-bedded conglomerate (northern part of deposit, Fig. 4), sandstone, and gray shale (Sangestan Formation) of late Jurassic to early Cretaceous age (Nabavi, 1972). Outcrops of unaltered conglomerate and sandstone are dark brown (in the southern part) whereas altered outcrops show various shades of grey to green. These Mesozoic sedimentary rocks were overlain by a series of Eocene rhyolitic to rhyodacitic tuffs and lavas in the northern and

southern parts of the area (Fig. 4). Sedimentary and rhyolitic/rhyodacitic rocks were intruded by granites (K/Ar 30 Ma; Zarasvandi et al., 2004) and relatively more mafic granitoids consisting of quartz monzodiorite-granodiorite (K/Ar 14 ± 4.6 Ma; Zarasvandi et al., 2004). The granites show graphic and equigranular textures, whereas the younger intrusions are porphyries with a fine-grained matrix. Hypogene Cu mineralization at Ali-Abad is hosted largely by a ~15 Ma old granitoid stock and, to a lesser extent, by an aureole of contact-metamorphosed conglomerate and sandstone.

Alteration

In outcrops and drillcores, potassic alteration occurs as pervasive and fracture-controlled replacement of primary minerals of the younger porphyritic granitoids by Mg-rich biotite, K-feldspar, and quartz, accompanied by chalcopyrite, pyrite, and magnetite. Most of the alteration biotite is fine grained and replaces minerals in the matrix of the

rocks as well as ferromagnesian and plagioclase phenocrysts. The large (0.5–1 cm) plagioclase phenocrysts are altered to K-feldspar along their rims. Phyllic alteration zones are distributed in the western part of the Darreh-Zerreshk area; this alteration is characterized by the replacement of almost all rock-forming silicates by sericite and quartz, and it overprints the potassic and propylitic zones. Quartz veinlets are associated with sericite, pyrite, chalcopyrite, and magnetite. Phyllic overprinting of the potassically altered rocks changed the plagioclase and orthoclase to sericite, and the biotite to chlorite. Propylitic alteration is defined here as the development of assemblages containing epidote with minor amounts of chlorite, calcite, and locally actinolite. These alteration minerals replace primary amphibole and plagioclase. Propylitic alteration forms a halo around the potassic and mineralized zone. A localized argillic zone represents the latest hydrothermal stage of alteration in the Darreh-Zerreshk area. The distribution of this alteration is controlled by faults that in turn localize preferentially eroded gullies. An advanced-argillic alteration zone was defined by plotting in the map the field localities of all samples that were analyzed by X-ray diffraction (XRD) by Dehghani (2000). Rocks of the advanced argillic zone are very soft, yellow to white, and consist of assemblages of kaolinite and pyrophyllite, associated with gypsum, hematite, limonite, and chalcocite.

Potassic alteration was not detected at the surface in the Ali-Abad area. An alteration mineral assemblage consisting of quartz, chlorite, and epidote, which are indicative of propylitic alteration, characterizes samples of granodiorite–quartz monzodiorites and of volcanic rocks. These alteration zones occur mainly in the northeast and southwest sections of the area (Fig. 4). The most conspicuous alteration at Ali-Abad is phyllic alteration. The granites and some of the volcanic rocks have undergone intense but irregular phyllic alteration. Portions of the granitic rocks exhibiting phyllic alteration were intensely brecciated and include minor stockwork-style sulfide and supergene Fe-oxide mineralization. An argillic alteration assemblage consisting mainly of quartz, kaolinite, and montmorillonite, with minor sericite, occurs in volcanic rocks in the northern part of the mapped area (Fig. 4). Field observations indicate that argillic alteration zones are adjacent to, and overprint, phyllic alteration zones.

Mineralization

Table 1 summarizes and contrasts the geologic, alteration, and mineralization features of the Darreh-Zerreshk and Ali-Abad deposits; the deposits are very similar. Exposed mineralization at the Darreh-Zerreshk deposit is limited to a thick (20–50 m) layer of oxidized Cu ores overlying the hypogene ore, with a transitional supergene enrichment zone in between. At depth (more than 80 m), hypogene sulfides occur as disseminations, mostly in veinlets, and veins in the potassic alteration zone, and in lesser concentrations in the phyllic alteration zones. In the potassic alteration zone, hypogene sulfide minerals are mainly chalcopyrite and bornite with subordinate magnetite and pyrite; these minerals are associated with biotite and quartz-K-feldspar veins. Oxidized ores are significant in the Darreh-Zerreshk deposit, where the oxidized zone has a development of 20 to 50 m from the surface. It includes mainly malachite, azurite, cuprite, chrysocolla, and native copper as ore minerals. A thin leached gossan is located in the upper parts of oxidized zone along the faults and fractures (Fig. 3). Hematite, limonite, goethite, and turquoise are common minerals in Darreh-Zerreshk leached caps. Mixed sulfides and oxidized minerals such as cuprite, native copper, chalcocite, and covellite characterize a transitional zone with limited supergene enrichment. The occurrence of native Cu and cuprite may suggest that this is a fossil supergene zone undergoing oxidation.

In the Ali-Abad deposit, the mineralized zone is restricted to a 40–50 m oxidized and supergene enriched zone overlying the hypogene sulfide zone. Chalcopyrite, pyrite, magnetite, and bornite assemblages are associated with potassic alteration from an early hydrothermal stage. Chalcopyrite and minor amounts of molybdenite occur within quartz veins both in potassically and phyllically altered rocks. Ilmenite, magnetite, and hematite are present as disseminated mineralization within phyllic and argillic alteration in granitic rocks. The highest grade portions of the hypogene zone are characterized by intense phyllic alteration. The supergene zone has a wide horizontal extension, and contains sooty chalcocite and covellite. On top of the supergene zone at Ali-Abad is an intensely leached cap about 10 m in thickness, but it is less well developed than in the Darreh-Zerreshk deposit.

In addition to the mineralization in granitoids, thin veinlets of chrysocolla, malachite, azurite, and oxides with remnant pyrite fill fractures within

argillized volcanic rocks (rhyolitic-rhyodacitic tuffs). They provide evidence of more extensive low-grade hypogene mineralization, only indicated by the colorful oxides.

Structure

Two questions posed at the beginning of this study were: (1) What relationship do the mineralized stocks and the mainly fracture-controlled mineralization have with regional structures? And (2), how did the fracture patterns evolve with time, in terms of pre-ore, ore-stage, and post-ore events? Therefore, our structural studies focused on larger faults at the regional scale, on mineralized faults and joints, and any post-ore structures in both deposits. As indicated above, the study area is located at the juxtaposition of the edge of the Central Iranian block and the CIVPB (Fig. 1). The Darreh-Zerreshk and Ali-Abad areas are restricted in the west by CIVPB volcanic rocks and the Dehshir-Baft fault, and in the east by Paleozoic to Jurassic rocks of the Central Iranian block (Fig. 1). The regional Dehshir-Baft dextral strike-slip fault is the major structural feature farther to the west and southwest of the study area (Fig. 1). The regional Dehshir-Baft dextral strike-slip fault is about 350 km in strike length, and follows roughly the NW-SE trend of the CIVPB. The regional strike of the Dehshir-Baft fault varies from about N20°W at its northwestern end—south of the city of Nain—to about N50°W at its southeastern termination, northwest of the town of Sirjan (Berberian, 1976). This fault is still tectonically active; it initially developed in Cretaceous time and has continued to move episodically until the Recent, as evidenced by displacement of Quaternary gravels. As a result of dextral strike-slip displacement, Cretaceous limestones (Taft Formation) southwest of Yazd Province, including those in the Darreh-Zerreshk and Ali-Abad area, have moved 50 km southeastward to be juxtaposed against volcanic rocks across this fault (Berberian, 1976).

The major Dehshir-Baft strike-slip fault system was partitioned into several parallel shear zones, transtensional pull-apart basins, and other syntectonic structures in southwestern Yazd Province and southwest of the Iranian copper province. In general, all of the structures in this area have been influenced by “Alpine” age effects that can be associated to the Dehshir-Baft fault. The pull-apart basins that developed between parallel shear zones in this area and in the central Iranian volcano-plutonic belt may have localized the shallow

TABLE 1. Geology and Mineralization of the Darreh-Zerreshk and Ali-Abad Porphyry Copper Deposits

Deposit	Rock type	Wall rock	Alteration zoning	Age	Sulfide minerals	Ore structure	Metallic type
Darreh-Zerreshk	Quartz diorite	Eocene tuff	Potassic, sericite,	Oligo-Miocene	Chalcopyrite + pyrite + chalcocite bornite + magnetite covellite	Veinlet disseminated	Cu, Mo, Au, Ag
	Quartz monzodiorite	Cretaceous limestone	argillic, and propylitic				
	Tonalite and granite						
Ali-Abad	Alkali-granite			Oligo-Miocene	Chalcopyrite + pyrite + chalcocite + molybdenite + galena + sphalerite	Veinlet disseminated	Cu, Mo, Ag
	Granodiorite	Eocene dacite to	Sericite, argillic				
	Quartz monzodiorite	Rhyodacite tuff	Propylitic				

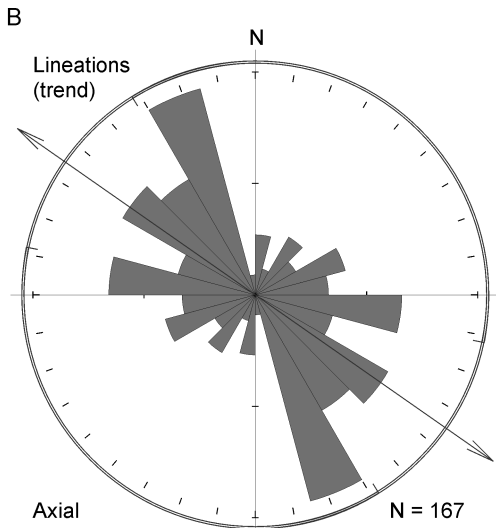
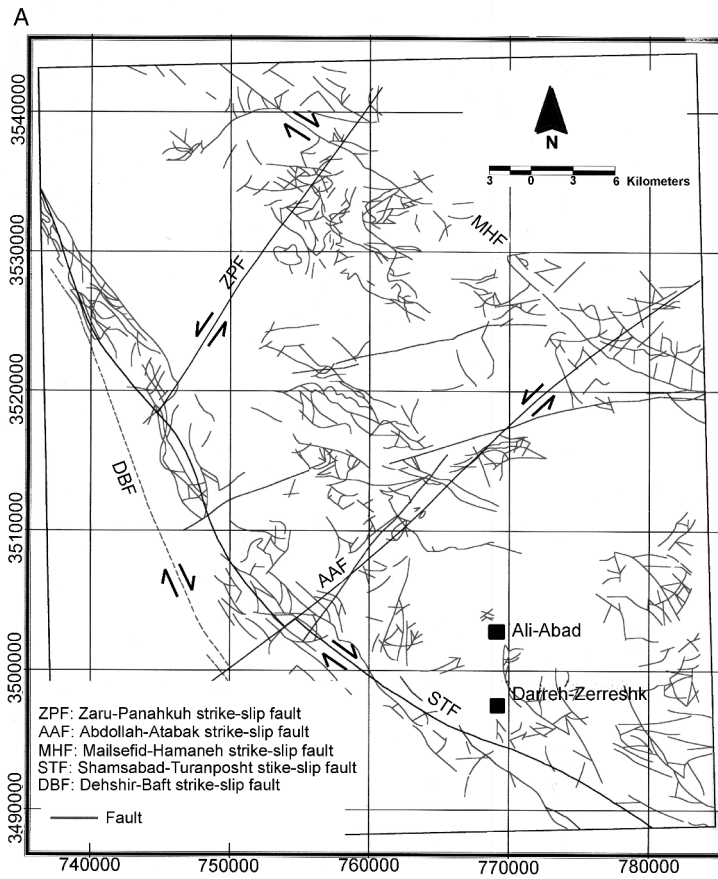


FIG. 5. A. Regional fault/fractures map of southwestern Yazd based on Landsat TM images, field observations, and geophysical data. B. Rose diagram of measured faults/fractures in this area. Some named structures are from Hajmolaali and Alavi (1993).

could have focused granitoid porphyry magmatism, and controlled the formation of the Darreh-Zerreshk and Ali-Abad porphyry copper deposits. Mapping of faults and fractures of southwestern Yazd Province were undertaken on the basis of Landsat images, geophysical maps, and field observations (Fig. 5A). All faults southwest of Yazd have a predominant trend of N20°–35°W, which is parallel to the trend of the Dehshir-Baft strike-slip fault (Fig. 5B).

In the study area, one can recognize four classes of faults/fractures: (1) the oldest faults/fractures are NNW-SSE-trending structures, mostly distributed in Paleozoic and Mesozoic rocks. This group is the most prominent in terms of frequency; its structures are parallel to, and have similar dextral motions as,

emplacement of magmas, as has been suggested for other orogenic belts (e.g., Richards et al., 2001). It appeared important to test whether these structures

to the main Dehshir-Baft fault (DBF). (2) The second class of structures comprises NW-SE-trending faults/fractures. These are the most conspicuous in terms of length, and are primary faults related to the DBF. These groups are synthetic to, and have similar dextral displacements as, the DBF, but strike approximately $N55^{\circ}W$. The linear contacts between alluvial plains and volcanic-plutonic rocks are characterized by these faults, which therefore control much of the landscape. Most of the known mineralization, such as at the Darreh-Zerreshk and Ali-Abad porphyry copper deposits, is located in the intervening domains between $N55^{\circ}W$ -trending faults. (3) The third group consists of NE-SW-trending faults/fractures, which have sinistral strike-slip displacements and are antithetic to the main DBF. These faults cut all of the rocks in the study area.

(4) The fourth group are N-S-trending faults/fractures, which have sinistral strike-slip motions with 500 to 1000 m of normal dip-slip (oblique) displacements. They are essentially transtensional faults that impart N-S-trending valley structures to the southern and central parts of the study area. The low-relief areas of the landscape located along these extensional faults are in places filled with thick accumulations of clastic sediments. Most of the intrusive bodies in the area are located along, and show elongation parallel to, these extensional structures.

These four classes of faults/fractures can be interpreted to constitute conjugate shears to the main DBF shear. Fault measurements in both deposits show four sets of faults at Darreh-Zerreshk and Ali-Abad (Figs. 6A and 6B). These are: (A) NE-SW-trending faults; (B) WNW-ESE-trending faults; (C) NW-SE-trending faults; and (D) E-W-trending faults (better developed at Darreh-Zerreshk). More than 50% of all faults observed in both deposits show dips between 70° and 80° . All of the NE-SW-trending faults (Type A) are associated with alteration (phyllic and argillic) and are mineralized to some degree. Mineralized faults show sinistral-normal (oblique) displacements; the average strike of mineralized faults is $N5^{\circ}-35^{\circ}E$. Faults/fractures with NW-SE (Type C) and WNW-ESE trends (Type B) and exhibiting evidence for dextral motion are generally barren faults; they most probably postdate the mineralization. Steeply dipping fault planes and shallowly plunging slickensides suggest that fault/fracture systems in both deposits are associated with the secondary fault systems of the regional DBF system. Frequency, distribution, and reactivation of

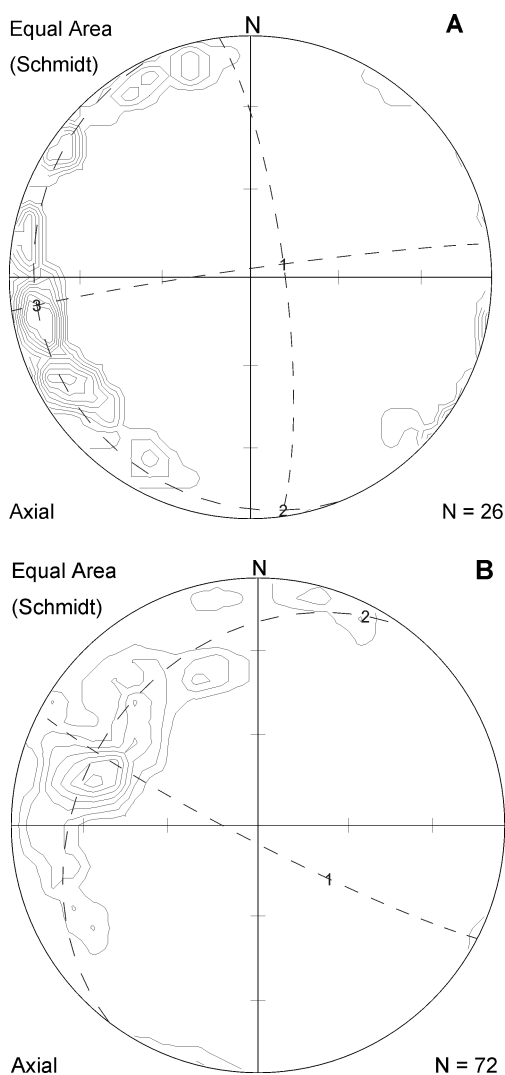


FIG. 6. Schmidt lower hemisphere stereoplots of faults in the Darreh-Zerreshk (A) and Ali-Abad (B) deposits.

faults in the area have enhanced permeability and oxidation, thus promoting development of the enrichment blankets (especially in the Ali-Abad deposit), which are important with regard to the economic feasibility of the deposits.

Lower equal-hemisphere diagrams of mineralized joints within intrusive, volcanic, and sedimentary host rocks associated with sulfide veinlets at Ali-Abad and Darreh-Zerreshk show that the strike of mineralized joints is $N5^{\circ}-35^{\circ}E$ (average $N20^{\circ}E$), which are here interpreted to be tensional joints

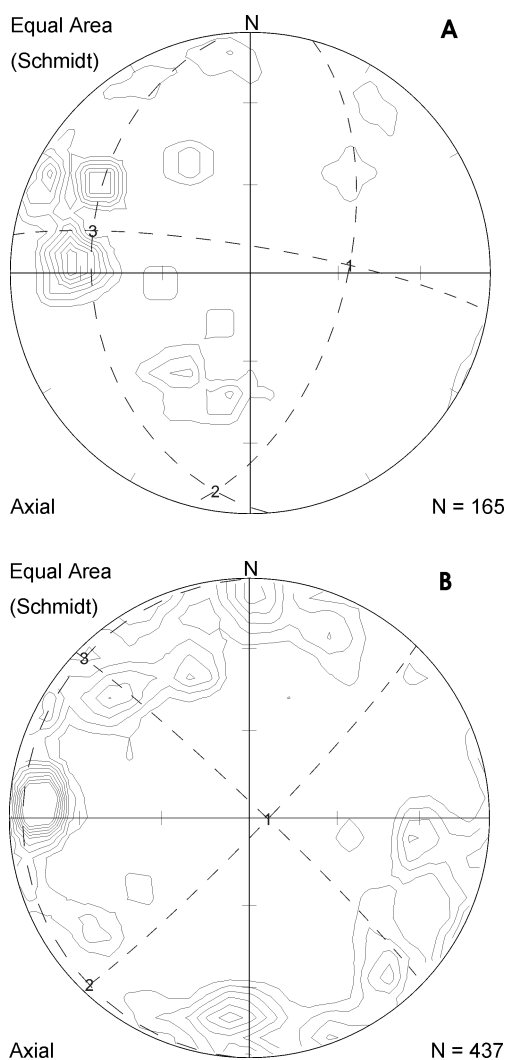


FIG. 7. Schmidt lower hemisphere stereoplots of joints in the Darreh-Zerreshk (A) and Ali-Abad (B) deposits.

(Figs. 7A and 7B). This strike is similar to the strike of mineralized faults, quartz monzodiorite-granodiorite dikes ($N35^{\circ}E$), and the regional pattern of faults. These data suggest that the Dehshir-Baft dextral strike-slip fault as a principal deformation zone (PDZ) has created three generations of faults/fractures and mineralized faults/fractures that are parallel to a N-S to NE-SW axis of maximum compressive stress. Tensional gashes or pull-aparts tend to form parallel to the σ_1 - σ_2 plane and perpendicular to σ_3 (e.g., Riedel, 1929). The preferred orien-

tation of mineralized fractures in the deposits is so well developed that it must impart a marked anisotropy to the distribution of Cu ore grades, which should be considered during reserve calculation and mine planning (e.g., Lindsay, 1997).

In summary, the development of second-order faults to the Dehshir-Baft dextral regional fault (DBF) and of parallel shear structures is interpreted to be synchronous with the emplacement of granitoid intrusions in the two deposits and southwest of Yazd. The second family of faults resulted from motion of the DBF, and third-order faults/fractures played an important role in the localization and hydrothermal circulation within the Darreh-Zerreshk and Ali-Abad deposits. If the deformational history of the area can be explained as a protracted period of deformation resulting from a relatively consistent prevailing stress regime, the faults/fractures (and associated joints) in these deposits and mapped area (Figs. 5–7) are geometrically consistent with a simple shear model of a dextral transcurrent (strike-slip) fault system (e.g., Woodcock and Schubert, 1994). According to this model, the regional DBF would represent the principal deformation zone (PDZ). The NW-SE-striking major faults, and NNE-SSW- and N-S-striking major faults are interpreted to represent secondary Riedel (P, R, and R') and tensional structures. In Figure 5, the faults/fractures located at angles between 10° and 20° from the PDZ are synthetic (R) structures and the faults/fractures at angles higher than 70° from the PDZ are antithetic structures (R'). The faults at angle $-\alpha/2$ from the PDZ are P structures. In the study area, P structures with $N55^{\circ}W$ strike are the most important factors for the formation of secondary parallel shear zones and small pull-apart basins.

In summary, this structural study suggests that Darreh-Zerreshk and Ali-Abad intermediate to mafic granitoid intrusions were emplaced along collected tensional gashes or a pull-apart structure in a secondary shear zone related to the dextral DFB system (Fig. 8). On the basis of this model, formation of these porphyry deposits was coeval with the evolution of a dextral transcurrent fault and formation of tensional structures between two secondary (p) faults.

Igneous Petrology

Both the Darreh-Zerreshk and the Ali-Abad copper deposits are spatially associated with quartz-

monzodiorite, granodiorite, and granite porphyry stocks intruded into sedimentary and volcanic rocks. Several barren stocks occur to the south and southwest of the mineralized area (e.g., Hassan-Abad, Touranposht, and southeastern part of Hassan-Abad stocks). In areas that have not been too deeply eroded, magmatic sequences commence with extrusive basalt, andesite, dacite and rhyolite (Dehghani, 2000). Field observation shows that volcanism was followed by intrusion of the following rock types, from older to younger:

Granites are the oldest intrusions, and the major component of the intrusive complex of the Ali-Abad area (Fig. 4); the contact between quartz monzodiorite–granodiorite and granite is sharp, as seen in the field and in drill holes. The equigranular granite shows graphic texture and consists of mainly of K-feldspar, quartz, and minor amphibole. The other minerals in these rocks are zircon, apatite, magnetite, ilmenite (minor), and sulfides. Clay minerals and sericite (muscovite) are secondary alteration products.

Granodiorite porphyries consist of 60–70 vol% of plagioclase (An15–22; 1–5 mm). The other main phenocrystic phases are quartz, orthoclase, amphibole, and biotite. Feldspars have been extensively saussuritized (clay, sericite, muscovite), but relict plagioclase twinning can be observed. Quartz phenocrysts tend to be euhedral to subhedral and show apatite and glass inclusions. The most important amphibole mineral is green hornblende. Hornblende crystals are euhedral and have been partially altered to epidote, chlorite, and biotite. Apatite, sphene, zircon, and opaque minerals are common accessory phases in granodiorite porphyritic rocks.

Quartzmonzodiorite porphyries contain more than 50 vol% phenocrysts consisting of twinned and zoned plagioclase, and highly altered amphibole. The matrix is fine-grained and consists of plagioclase, minor quartz, amphibole, and biotite; plagioclase occurs either as isolated phenocrysts or as glomerocrysts, and they are variably altered to a clay, calcite, sericite, and epidote. Secondary quartz is always anhedral and occurs in fractures and veins, where it shows undulatory extinction, attesting to the effects of strain. In drillcore samples, amphibole crystals are euhedral to subhedral and altered to chlorite, epidote, and biotite. Primary biotite is stubby and subhedral, with a dark brown to yellowish color; it is distinguished from secondary biotite by shape and the fact that secondary biotite has less developed cleavage and is green to red in color. The

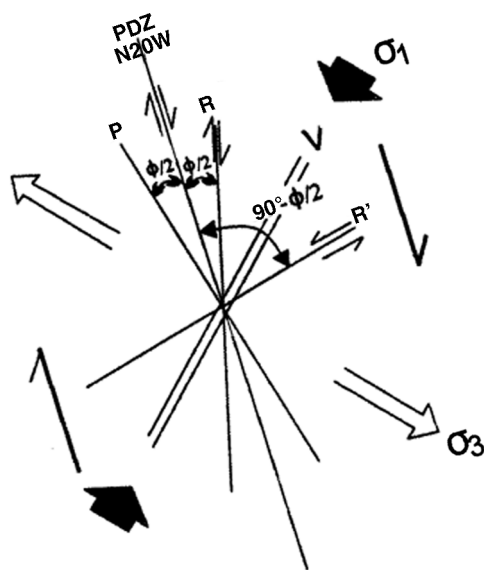


FIG. 8. Schematic proposed model for tectonic pattern of the Darreh-Zerreshk and Ali-Abad areas in the simple-shear system (Riedel, 1929).

principal opaque phases in these rocks are magnetite, chalcopyrite, and pyrite. Enclaves of microgranular diorite are common within the quartz monzodiorite–granodiorites in the Ali-Abad area and southeast of Darreh-Zerreshk. Enclaves are egg-shaped masses ranging in size from a few millimeters to centimeters, and they characteristically are formed predominantly of plagioclase and amphibole.

Dacite–rhyolite bodies are not related to the mineralized porphyries. These are subvolcanic rocks of Eocene age, and occur as small outcrops in the study area north of Ali-Abad and Darreh-Zerreshk (Fig. 2). These felsic rocks exhibit porphyritic textures with phenocrysts of feldspar and quartz, embedded in a matrix of similar mineralogical compositions.

Geochemistry

Major elements

Whole-rock major- and trace-element data, including rare-earth elements (REE), for all the intrusions in the study area are presented in Table 2. Modal QAP values calculated from chemical analyses (Streckeisen and Lemaitre, 1979) confirm that rock compositions in the mapped area range from

TABLE 2. Whole-Rock Major (wt%) and Trace Elements (ppm) from Igneous Rocks in the Study Area¹

Sample no.:	DZ-38	MN34-1	MN34-2	MN34-40	MN34-21	MN34-68	MN34-78	MN34-79	MN34-80
Rock:	gr	gr	gdr	qz-di	gdr	gdr-qmdi	gdr	gdr-qmdi	gdr-qmdi
Major elements, %									
SiO ₂	71.59	74.81	69.02	59.85	71.32	62.48	65.42	65.24	66.27
TiO ₂	0.303	0.333	0.29	0.635	0.315	0.58	0.53	0.617	0.49
Al ₂ O ₃	15.28	13.15	14.34	14.89	14.15	15.08	14.61	15.05	15.09
Fe ₂ O ₃	2.29	2.01	2.06	4.08	1.6	2.35	1.48	2.45	3.67
MnO	0.008	0.04	0.007	0.037	0.038	0.026	0.034	0.026	0.02
MgO	0.34	0.97	0.79	2.23	1.05	1.44	1.1	1.65	1.1
CaO	2.94	1.9	1.87	5.35	4.05	6.33	4.86	4.96	4.15
Na ₂ O	2.94	1.74	2.23	2.7	2.23	2.47	2.04	2.07	3.21
K ₂ O	3.39	3.6	3.65	3.86	3.39	2.19	6.34	3.73	2.53
P ₂ O ₅	0.125	0.099	0.12	0.347	0.097	0.26	0.137	0.255	0.206
LOI	0.34	0.71	4.41	5.62	0.93	6.35	3.14	3.23	2.68
A/CNK	1.1	1.5	1.3	0.82	0.96	0.84	0.73	0.91	0.97
Total	99.54	99.36	98.78	99.59	99.17	99.55	99.69	99.27	99.41
Trace elements, ppm									
Rb	47	59	61	66	56	41	96	63	45
Ba	908	1023	883	967	845	788	788	1526	990
Th	9	3	11	14	11	9	16	12	10
U	5	1	3	4	5	1	4	1	1
Nb	7	4	7	8	6	15	7	9	7
La	14.3	11	17.8	41.1	20	32	17.5	32.3	26.4
Ce	24.8	19.4	29	78.9	31.9	64.1	27.9	53.3	46.1
Pb	30	56	32	33	61	37	37	35	32
Pr	2.91	2.28	3.43	9.8	3.56	10.2	3.98	7.64	6.19
Mo									
Sr	746	611	574	1659	615	993	572	734	996
Nd	10.7	8.46	12.9	38.2	13.3	38.4	15.2	29.3	22.2
Sm	1.89	1.61	2.2	6.85	2.2	7.1	3.02	5.21	3.83
Zr	105	103	102	234	101	128	133	158	183
Eu	0.67	0.61	0.73	2	0.74	1.77	1.16	1.56	1.24
Gd	0.9	0.77	1.07	3.23	1	3.26	1.5	2.52	1.8
Tb	0.17	0.14	0.22	0.6	0.18	0.59	0.29	0.45	0.35
Dy	0.78	0.6	0.93	78.9	0.79	2.71	1.37	1.98	1.59
Y	12	12	13	16	12	14	17	16	14
Ho	0.18	0.13	0.21	0.51	0.16	0.49	0.25	0.33	0.27
Er	0.52	0.38	0.57	1.36	0.45	1.32	0.68	0.92	0.78
Tm	0.07	0.05	0.07	0.17	0.006	0.19	0.1	0.12	0.12
Yb	0.5	0.38	0.47	0.99	0.4	1.21	0.58	0.7	0.74
Lu	0.09	0.05	0.07	0.14	0.06	0.16	0.09	0.11	0.11
V	44	44	43	107	42	59	51	61	74
Cr	1	1	1	5	2	3	3	2	1
Ni	6	1	1	10	1	1	1	1	2
Cu	456	2554	1440	901	1883	622	1508	1735	157
Zn	49	87	146	76	86	86	40	56	63
S	13	14	9	211	531	280	658	324	5
Eu/Eu*	1.57	1.67	1.47	1.3	1.52	1.12	1.66	1.317	1.44
(La/Yb) _n	19.32	19.56	25.59	28.06	33.8	17.87	20.39	31.187	24.11

Table continues

TABLE 2. *Continued*

Sample no.:	AY-1	AY-2	AY-3	AY-4	AY-5	AY-13	AY-14	AY-21	AY-26
Rock:	alk-gr	alk-gr	alk-gr	alk-gr	alk-gr	gdr-qmdi	gdr-qmdi	gdr	alk-gr
Major elements, %									
SiO ₂	76.66	76.21	74.61	73.14	74.06	67.58	68.07	65.04	75.85
TiO ₂	0.178	0.192	0.178	0.198	0.169	0.42	0.396	0.326	0.2
Al ₂ O ₃	14.57	14.96	16.81	17.22	17.04	15.36	14.98	17.14	14.51
Fe ₂ O ₃	0.93	0.65	1.15	1.81	1.95	3.47	3.33	3.36	0.63
MnO	0.001	0.001	0.001	0.002	0.001	0.063	0.061	0.07	0.009
MgO	0.42	0.46	0.61	0.75	0.5	1.87	1.91	1.36	0.28
CaO	0.34	0.34	0.34	0.24	0.15	4.72	4.81	4.12	0.3
Na ₂ O	4.31	3.88	0.26	0.23	0.25	3.79	3.41	3.78	5.94
K ₂ O	1.45	1.95	4.36	4.71	4.26	1.73	1.87	2.19	0.54
P ₂ O ₅	0.039	0.041	0.044	0.042	0.035	0.216	0.184	0.18	0.051
LOI	0.59	0.83	1.01	0.84	0.69	0.74	0.75	2.21	1.52
A/CNK	1.5	1.7	3.2	3.2	1.06	1	1	1.06	1.4
Total	99.48	99.51	99.37	99.18	99.1	99.95	99.77	99.77	99.83
Trace elements, ppm									
Rb	51	59	121	125	110	52	58	45	14
Ba	145	213	201	274	205	746	696	822	6
Th	7	10	14	16	10	4	1	11	9
U	3	2	4	8	4	1	1	5	4
Nb	12	13	11	11	11	8	4	4	10
La	6.7	12.3	8.9	4.9	2.6	23.1	20.4	19.2	48.6
Ce	14.3	26.4	18.8	11.3	6.1	39.2	35.5	32.4	87
Pb	12	14	26	6	7	20	19	34	19
Pr	2.14	3.53	2.5	1.76	5.39	5.39	4.77	4.47	10.6
Mo									
Sr	144	89	18	46	15	883	815	1592	683
Nd	8.9	14.4	9.92	7.66	3.87	20.6	18.2	16.7	35.4
Sm	2.06	3.29	2.2	2.02	1.01	3.52	3.18	2.98	6.43
Zr	197	162	178	173	155	143	134	204	143
Eu	0.47	0.34	0.25	0.29	0.15	1.23	1.06	1.24	0.58
Gd	0.99	1.63	1.12	1.11	0.63	1.6	1.44	1.5	2.88
Tb	0.17	0.29	0.21	0.25	0.15	0.27	0.24	0.27	0.44
Dy	0.69	1.15	0.91	1.08	0.77	1.17	1.01	1.26	1.47
Y	15	19	21	22	19	13	12	9	33
Ho	0.15	0.22	0.22	0.26	0.18	0.23	0.22	0.29	0.26
Er	0.37	0.56	0.56	0.68	0.49	0.64	0.57	0.84	0.71
Tm	0.04	0.07	0.08	0.08	0.07	0.08	0.08	0.12	0.07
Yb	0.26	0.42	0.41	0.51	0.37	0.51	0.49	0.7	0.73
Lu	0.04	0.05	0.06	0.07	0.06	0.07	0.07	0.1	0.06
V	26	23	25	28	28	61	58	62	23
Cr	1	1	1	1	1	1	2	4	1
Ni	1	5	5	13	5	1	7	12	10
Cu	254	55	147	10394	1028	24	5	36	7
Zn	35	26	25	22	20	58	64	96	20
S	10	9	8	11	7	12	15	15	16
Eu/Eu*	1.07	0.44	0.48	0.56	0.57	1.58	1.51	1.53	4.12
(La/Yb) _n	17.41	19.79	14.67	6.49	4.75	30.613	28.14	18.53	44.99

Table continues

TABLE 2. *Continued*

Sample no.:	DH-8	DZ-36	MN34-92	AY-22	AY-65	AY-66	AH1-1	AH1-2	AH1-4
Rock:	alk-gr	gr	qz-di	gdr-qmdi	alk-gr	alk-gr	gdr	alk-gr	gdr
Major elements, %									
SiO ₂	74.83	74.74	57.63	69.16	77.83	79.18	62.68	71.06	67.45
TiO ₂	0.152	0.34	0.6	0.362	0.123	0.137	0.372	0.108	0.37
Al ₂ O ₃	15.09	13.48	14.4	15.16	12.23	11.77	20.49	16.61	16.66
Fe ₂ O ₃	0.78	1.8	3.05	3.66	0.57	0.98	3.8	3.45	2.94
MnO	0.011	0.01	0.07	0.168	0.004	0.007	0.026	0.052	0.04
MgO	0.19	0.85	1.92	1.32	0.21	0.23	1.5	0.52	1.84
CaO	0.37	2.29	10.5	2.46	0.38	0.41	1.01	0.12	2.15
Na ₂ O	2.7	2.37	2.94	4.31	3.84	5.95	1.63	0.38	5.06
K ₂ O	4.68	2.73	2.37	3.07	4.51	0.71	4.08	4.02	1.18
P ₂ O ₅	0.102	0.11	0.27	0.148	0.093	0.093	0.241	0.15	0.22
LOI	1.01	0.55	5.66	0.5	0.3	0.5	3.18	2.59	1.09
A/CNK	1.7	1.1	0.54	1.07	1	1.1	2.23	4	1.3
Total	99.91	99.27	99.41	100.318	100.09	99.96	99.009	99.06	99
Trace elements, ppm									
Rb	161	44	50	75	147	46	106	63	34
Ba	295	833	689	1083	518	16	577	648	399
Th	12	7	5	2	2	5	2	2	3
U	5	1	9	1	1	1	1	1	5
Nb	13	4	8	9	13	17	4	9	4
La	16.5								
Ce	34.2								
Pb	157	24	33	63	87	9	170	29	21
Pr	5.11								
Mo				1	1	1	9	13	13
Sr	696	740	932	823	65	85	127	96	624
Nd	19.1								
Sm	5.05								
Zr	90	114	121	127	88	130	74	69	72
Eu	0.58								
Gd	3.19								
Tb	0.75								
Dy	3.59								
Y	38	12	16	15	29	25	7	23	8
Ho	0.77								
Er	2.1								
Tm	0.28								
Yb	1.57								
Lu	0.22								
V	22	47	59	54	21	24	25	34	26
Cr	1	1	1	25	34	29	96	157	97
Ni	12	3	8	16	17	14	7	11	13
Cu	21	2260	2318	25	35	44	1183	182	523
Zn	110	76	70	3259	28	22	550	117	124
S	15	11	1184	281	78	54			
Eu/Eu*	0.44								
(La/Yb) _n	7.102								

Table continues

TABLE 2. *Continued*

Sample no.:	AH1-12	AH1-16	AH1-18	AH1-19	AH1-22	AH1-25	AH1-27	AH1-28	AH1-35
Rock:	gdr-qmdi	gdr	alk-gr	alk-gr	alk-gr	gdr-qmdi	alk-gr	gdr	alk-gr
Major elements, %									
SiO ₂	66.6	65.07	72.44	72.4	75.29	66.1	75.21	63.17	71.73
TiO ₂	0.36	0.433	0.085	0.101	0.102	0.387	0.092	0.377	0.286
Al ₂ O ₃	17.73	18.63	16.47	15.92	14.79	18.12	15.47	19.15	15.74
Fe ₂ O ₃	2.81	3.34	2.71	0.86	1.24	2.68	1.23	2.82	3.33
MnO	0.051	0.048	0	0.001	0.001	0.026	0.001	0.019	0.001
MgO	1.3	1.63	0.5	0.26	0.44	1.51	0.52	2.02	1.23
CaO	2.14	2.82	0.05	0.06	0.11	2.02	0.04	1.86	0.01
Na ₂ O	5.48	5.45	0.27	0.78	0.53	4.94	0.46	5.11	0.22
K ₂ O	1.27	1.16	3.66	7.96	6.03	2.39	5.75	2.59	3.98
P ₂ O ₅	0.26	0.301	0.127	0.132	0.151	0.258	0.128	0.279	0.067
LOI	1.02	0.33	2.84	0.82	1.13	0.73	1.08	1.83	3.18
A/CNK	1.3	1.3	5.3	1.6	2.3	1.4	2.5	1.3	3.7
Total	99.02	99.21	99.15	99.29	99.81	99.16	99.81	99.22	99.77
Trace elements, ppm									
Rb	33	33	60	137	104	60	110	61	87
Ba	465	425	354	819	738	655	681	597	295
Th	1	1	1	9	5	2	4	1	3
U	7	6	2	7	4	6	5	6	2
Nb	5	4	8	10	11	5	9	5	7
La									
Ce									
Pb	18	18	20	43	49	22	46	26	66
Pr									
Mo	14	13	15	35	14	19	11	29	15
Sr	626	766	87	99	116	674	93	621	117
Nd									
Sm									
Zr	80	86	57	86	69	89	69	84	84
Eu									
Gd									
Tb									
Dy									
Y	10	11	28	40	33	10	33	7	15
Ho									
Er									
Tm									
Yb									
Lu									
V	19	33	30	28	45	16	24	28	34
Cr	82	107	168	150	179	87	149	126	156
Ni	12	17	8	5	7	13	7	11	18
Cu	234	296	108	2717	2474	2911	1097	2714	993
Zn	149	195	21	111	147	254	133	260	340
S									
Eu/Eu*									
(La/Yb) _n									

Table continues

TABLE 2. *Continued*

Sample no.:	AH2-2	AH2-5	AH2-7	AH2-8	AH2-22	AH2-25	AH2-26	AH2-33
Rock:	alk-gr	alk-gr	gdr-qmdi	gdr	alk-gr	alk-gr	gdr	alk-gr
Major elements, %								
SiO ₂	72.83	74.21	63.48	65.99	72.78	71.25	64.53	72.17
TiO ₂	0.179	0.183	0.337	0.305	0.144	0.172	0.394	0.179
Al ₂ O ₃	18.35	17.06	18.32	17.44	17.56	18.23	18.22	18.06
Fe ₂ O ₃	1.21	1.61	3.03	2.82	1.82	2.3	2.8	2.12
MnO	0.003	0.004	0.015	0.075	0.005	0.003	0.022	0
MgO	0.7	0.59	2.02	1.96	0.81	0.69	2.39	0.48
CaO	0.16	0.11	1.75	2.04	0.16	0.03	1.56	0.01
Na ₂ O	0.22	0.25	5.06	5.29	0.22	0.16	5.39	0.17
K ₂ O	4.45	4.53	2.89	2.11	4.45	4.24	1.71	4.19
P ₂ O ₅	0.199	0.127	0.273	0.233	0.163	0.044	0.225	0.044
LOI	0.79	1.2	2.62	1.44	1.54	2.31	2.11	2.09
A/CNK	4.2	4	1.3	1.1	4.25	5.25	1.5	5.25
Total	99.09	99.87	99.79	99.7	99.65	99.42	99.35	99.51
Trace elements, ppm								
Rb	108	117	65	44	125	101	39	95
Ba	243	287	1197	753	298	250	555	207
Th	11	8	3	2	6	6	2	5
U	9	7	5	6	5	4	5	4
Nb	11	10	5	5	10	10	3	11
La								
Ce								
Pb	11	16	44	29	22	13	28	14
Pr								
Mo	32	19	17	18	18	22	27	27
Sr	58	69	577	665	70	86	539	84
Nd								
Sm								
Zr	135	144	83	88	119	126	68	128
Eu								
Gd								
Tb								
Dy								
Y	60	38	6	8	36	31	7	30
Ho								
Er								
Tm								
Yb								
Lu								
V	26	39	28	41	38	29	34	28
Cr	147	148	113	94	154	117	82	117
Ni	8	6	12	11	6	7	9	6
Cu	152	128	63	566	1603	234	954	70
Zn	30	26	87	152	72	47	228	23
S								
Eu/Eu*								
(La/Yb) _n								

¹Abbreviations: gr = granite; gdr = granodiorite; qz-di = quartz diorite; qmdi = quartz monzodiorite; alk-gr = alkali-granite. Major and trace elements analyzed by XRF and REE by ICP-MS.

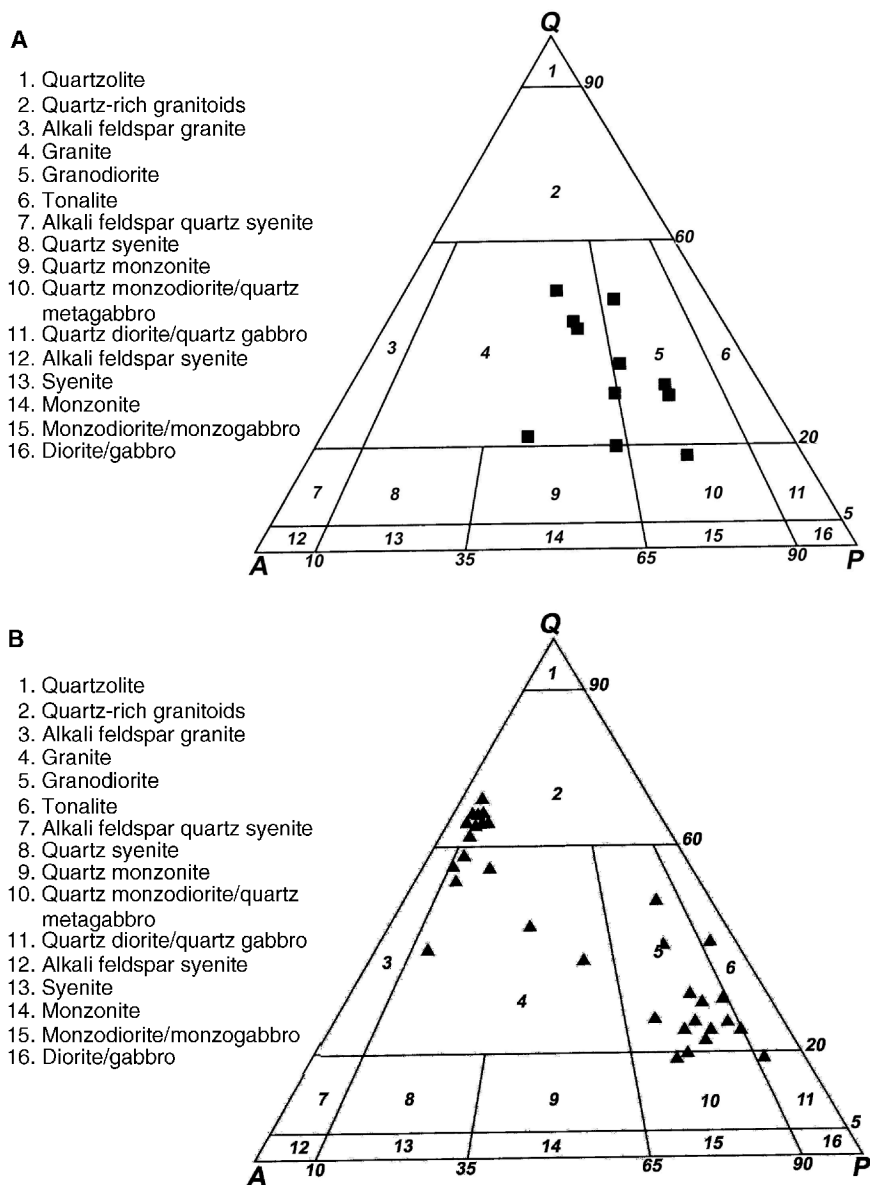


FIG. 9. Streckeisen and Lemaître (1979) Q(Quartz) A(Alkali-feldspar) P(Plagioclase) diagram showing classification of intrusion rocks in the study area in (A) Darreh-Zerreshk area (B) Ali-Abad area.

quartz-monzodiorite through granodiorite to tonalite (e.g., Hassan-Abad stock) to granite (e.g., Darreh-Zerreshk and Ali-Abad stocks; Figs. 9A and 9B). These igneous rocks have average A/CNK molecular ratios between 0.99 and 3. High A/CNK values for some of the samples are most probably the result of alteration (or crustal contamination), as suggested

by petrographic study, thus requiring caution when interpreting the major elements. From the geochemistry and consistent petrography, these rocks can be classified as I-type granitoids (e.g., Chappell and White, 1974). All analyzed rocks plot in the subalkaline field (Irvine and Baragar, 1971; Fig. 10), but it is evident that alkalis have been mobilized

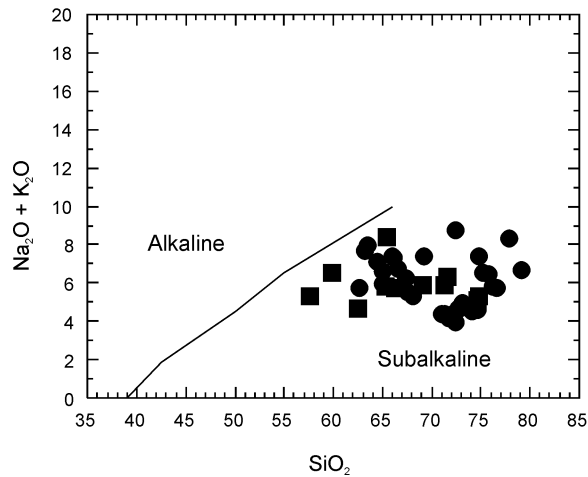


FIG. 10. SiO_2 (wt%) versus $\text{Na}_2\text{O} + \text{K}_2\text{O}$ (wt%) from Irvine and Baragar (1971) shows the subalkaline nature of intrusions in the Darreh-Zerreshk and Ali-Abad deposits. Symbols circles = Ali-Abad samples; squares = Darreh-Zerreshk samples.

during hydrothermal alteration and therefore cannot be used for petrogenetic classification. The overall range in SiO_2 in these rocks is from 54 to 75.3 wt%. Stocks with Cu mineralization are relatively more felsic, with a range in SiO_2 from 57 to 71 wt%, the high SiO_2 values probably due to silicification. A limited variation of major element compositions exists for the ore-bearing porphyries (Table 2). In least-altered samples (< 1% LOI) of quartzdiorite to granodioritic rocks, the K_2O content increases with increasing SiO_2 , whereas CaO , Al_2O_3 , MgO , TiO_2 , and Fe_2O_3 decrease, reflecting fractional crystallization of hornblende, plagioclase, and Mg-biotite.

Trace elements

REE patterns in granitoid complexes hosting Cu-porphyry mineralization are valuable tools in the elucidation of magma sources, and also to help assess the ability of magma to concentrate Cu. Trace elements and whole-rock REE data from all intrusion rocks in the study area have been normalized to chondrite and primitive-mantle abundance (e.g., Sun and McDonough, 1989). REE and trace elements are summarized below in spider diagrams for each area. The Darreh-Zerreshk granitoids display a steep pattern with average $(\text{La}/\text{Yb})_n$ values = 22.34, $(\text{La}/\text{Lu})_n$ values = 23.18, and Eu/Eu^* values = 1.30. This pattern with LREE enrichment and slightly positive Eu anomaly indicates that magma differentiation was controlled by hornblende fractionation

(e.g., Hanson, 1980; Nicolas and Harrison, 1980; Fig. 11A). The absence of a negative Eu anomaly may be due to high magmatic oxidation states (e.g., Nakamura, 1985; Lang and Titley, 1998; Richards et al., 2001) consistent with the abundance of magnetite in the rocks. Strong negative anomalies for Nb and Ti and positive anomalies for Pb are characteristic of arc magmas, and, when combined with their major oxides and chondrite-normalized REE pattern, support the classification of these rocks as derived from I-type calc-alkaline magmas (Fig. 11B).

The Ali-Abad granitoids display two different patterns in REE behavior (Fig. 12A). In general, they show a flat pattern, but geochemically they yield contrasting signatures, suggestive either of extreme fractionation effects or differing sources. The Ali-Abad equigranular granites (samples AY-1 to AY-5, AY-26 and AY-8) are characterized by HREE depletion and less LREE enrichment with strong negative Eu anomalies. In contrast, the younger (mineralizing) quartz monzodiorite-granodiorite rocks (samples AY-13, AY-14 and AY-21) are further enriched in LREE and slightly in HREE, plus a small positive Eu anomaly. Trace-element compositions of both rock types are shown in Figure 12B. Strong negative anomalies for Nb and Ti and positive anomalies for Pb and Sr suggest an I-type arc-like affiliation for these rocks. Moderate to strong negative Eu anomalies, ($\text{Eu}/\text{Eu}^* = 0.44\text{--}1.5$), associated with the flat middle to heavy REE pattern

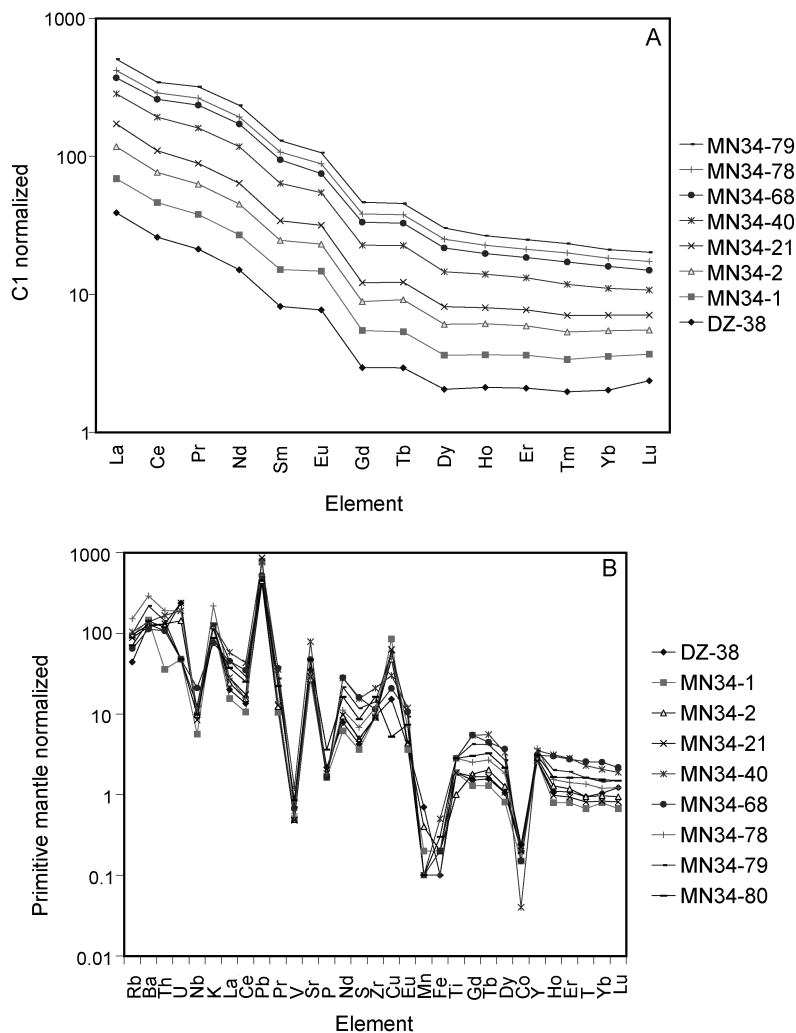


FIG. 11. Normalized REE (A) and trace-element (B) diagrams for the Darreh-Zerreshk granitoid intrusions. Normalized based on Sun and McDonough (1989) data. Sample numbers correspond to analyses in Table 2.

shows plagioclase fractionation during differentiation of these magmas. LREE-enrichment combined with the lack of an Eu negative anomaly ($Eu/Eu^* = 1.5$) and $(La/Yb)_n$ average values = 25.7 indicate that hornblende fractionation controlled differentiation of quartz monzodiorite-granodiorite parent magmas. Burnham (1979) estimated minimum magmatic water content of 3 wt% H_2O for crystallization of amphibole in silicate melts, but higher water contents (> 4 wt% H_2O) would be required for crystallization of hornblende as early phenocrysts (Nancy, 1933; Merzbacher and Egger, 1984).

In summary, trace elements and REE data for the study area allow us to infer: (1) Equigranular granitic rocks in the study area are I-type arc-granites, and they are thus very different from both the Jurassic Shir-kuh granites (S-type) and the intermediate to mafic Cu-bearing granitoids; granitic rocks such as the Ali-Abad stock were derived from a relatively drier magma and differentiated by plagioclase fractionation. (2) Quartz diorite to granodioritic rocks in the mapped area (such as the Darreh-Zerreshk stock) crystallized from relatively hydrous differentiated magmas, controlled by hornblende

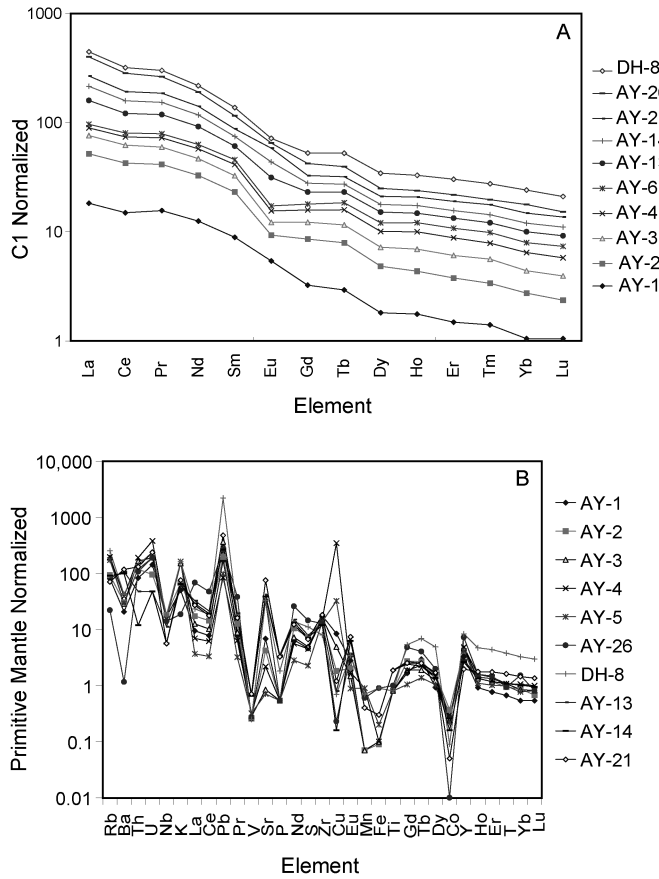


FIG. 12. Normalized REE (A) and trace-element (B) diagrams for the Ali-Abad granitoid intrusions. Normalized based on Sun and McDonough (1989) data. Sample numbers correspond to analyses in Table 2.

fractionation. Plots of Eu/Eu^* versus $SiO_2\%$ (Fig. 13) and $(La/Yb)_n$ versus $SiO_2\%$ (Fig. 14) and lack of significant negative Eu anomalies are compatible with the hypothesis that hornblende fractionation was the most important process in the petrogenesis of the mineralized intrusions. The quartz diorite–quartz monzodiorite–granodiorite porphyries associated with copper-mineralization at Darreh-Zerreshk and Ali-Abad are coeval, and show geochemical behavior similar to that of subduction-related granitoid plutonism hosting porphyry copper mineralization in the convergent environment elsewhere in the world (e.g., Maksiyev, 1990; Lang and Titley, 1998; Richards et al., 2001; Zengqian et al., 2003). In contrast, granitic rocks in both deposits are the oldest intrusions in the suite, and were formed in drier conditions by crystallization of plagioclase, crystal-

lized at relatively greater depth, and are unrelated to the relatively more mafic, porphyritic, mineralizing intrusions. Arc magmatic affinity and the enrichment in large ion lithophile elements (LILE, Ba, Rb, Sr, and K) in the studied rocks suggest that the source of the porphyry magmas can be a mixture of mantle and crustal materials (e.g., Miyashiro, 1977).

Discussion

Late Mesozoic and Cenozoic magmatic rocks in the central Iranian volcano-plutonic belt host several porphyry copper deposits. This magmatic belt defines a series of parallel tectonomagmatic zones (Fig. 1). Voluminous granitoid magmatism and strike-slip faulting are the most important tectonomagmatic features in the CIVPB. Where erosion has exposed the intrusive bodies and porphyry copper

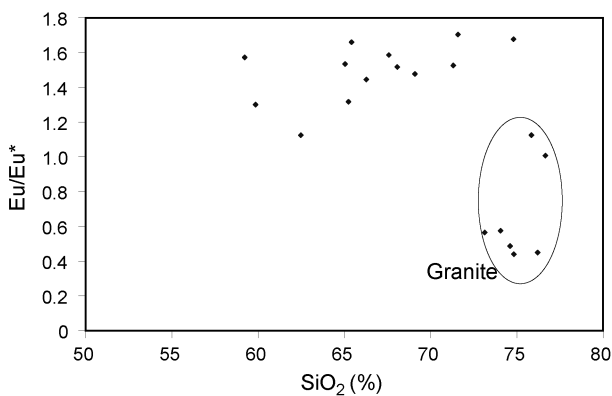


FIG. 13. Plot of Eu/Eu^* anomaly versus SiO_2 (wt%) for the Darreh-Zerreshk and Ali-Abad granitoid intrusions. Relatively older, barren, equigranular granites represent a distinct population (ellipse).

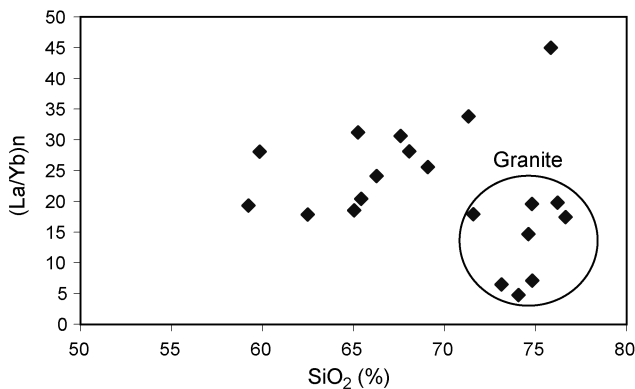


FIG. 14. Diagram of Cl-normalized $(\text{La}/\text{Yb})_n$ ratio versus SiO_2 (wt%) for the Darreh-Zerreshk and Ali-Abad granitoid intrusions. Normalized based on Sun and McDonough (1989) data. Relatively older, barren, equigranular granites represent a distinct population (circle). See text for discussion.

systems (e.g., the late Eocene–Miocene porphyry copper mineralization in Iran) a close relationship between magmatism and strike–slip faulting can be inferred, such as at fault intersections and parallel shear zones. The occurrence of porphyry copper-type and associated mineralization within this belt in relation to mappable structural zones suggests that the intersections of lineaments, strike-slip faults, and pull-apart basins provided flow paths for the ascent of arc granitoid magmas and their evolving hydrothermal plumes to crustal levels. In the central Iranian volcano–plutonic belt, spatial associations between parallel shear zones along strike-slip faults/fractures and porphyry granitoid magmas indicate that the largest of porphyry systems are structurally controlled (e.g., Sar-Cheshmeh deposit).

Magmatism in the central Iranian volcanoplutonic belt and especially in the study area was related to the Cenozoic magmatic arc, which occurred in response to relatively shallow and oblique subduction of the Arabian plate beneath the Iranian plate (e.g., Berberian and King, 1981; Alavi, 1994). We conclude that the geology, igneous petrology and geochemistry, alteration, mineralization, and structure of the Cu–Mo mineralization at Darreh-Zerreshk and Ali-Abad qualifies these two systems as typical porphyry Cu (Mo) deposits, formed in a transtensional environment. Arc magmatism in the study area is restricted to the Oligocene to late Miocene (Zarasvandi et al., 2004). Deep structural and tensional gashes or secondary pull-aparts control the distribution of these rocks.

TABLE 3. Comparison of the Darreh-Zerreshk and the Ali-Abad Deposits with Major Porphyry Copper Deposits in Iran

Characteristics of mineralization	Ali-Abad	Darreh-Zerreshk	Sungun	Sar-Cheshmeh
Tectonic setting	Continental magmatic arc	Continental magmatic arc	Continental magmatic arc	Continental magmatic arc
Volcanic rocks	Dacite to rhyodacite	Dacite to rhyodacite	Dacite to trachy-andesite	Andesite to trachyte
Intrusive rocks	Granite, granodiorite Quartz monzodiorite	Granite, granodiorite Quartz monzodiorite quartz diorite	Quartz monzodiorite granodiorite granite	Trachyandesite Granodiorite
Phyllic alteration	Abundant	Restricted	Abundant	Abundant
Stockworks	Abundant	Abundant	Abundant	Abundant
Silicification	Abundant	Abundant	Abundant	Abundant
Metallic types	Cu-Mo-Ag	Cu-Mo-Ag-Au	Cu-Mo-Ag-Au	Cu-Mo-Ag-Au

Magmatism in these structural environments was calc-alkaline and metaluminous to peraluminous in composition. Mineralogy and geochemistry of intrusive rocks are indicative of I-type granitoids in a typical volcano-plutonic arc setting.

The geochemistry of major elements and REE indicates that fractional crystallization of hornblende may have played the most important petrogenetic role in the evolution of differentiation of mineralized intrusions. A decreasing concentration of REE, steepening profiles, approximately greater upward concavity in heavy REE, and changes in the Eu anomaly from negative to either markedly less negative or positive are the best evidence for hydrous magmatism and high-oxidation state during hornblende fractionation (e.g., Lang and Tittley, 1998; Richards et al., 2001). The above features are documented for the mineralogy, major oxide, and rare-earth element compositions of the Darreh-Zerreshk and Ali-Abad porphyry granitoids. The styles of mineralization and alteration of both deposits are similar to those of the classical porphyry copper deposits (e.g., Lowell and Guilbert, 1970). The phyllic, propylitic, and argillic alteration occur in both deposits, with potassic alteration identified at

the surface of the Darreh-Zerreshk and at depth in the Ali-Abad deposit. Darreh-Zerreshk shows potassic and phyllic alteration with silicification and high-grade hypogene mineralization. The argillic alteration zone is fault controlled in both deposits, but it is more extensive in Ali-Abad. A supergene enrichment zone is restricted in both deposits, but a relatively shallow (about 40 m deep) cementation blanket with sooty chalcocite and covellite caps the Ali-Abad deposit.

The strike-length axis of granitoid stocks, development of alteration (especially phyllic alteration), and structural trends of mineralized fractures and dikes are compatible with the formation of Darreh-Zerreshk and Ali-Abad porphyry systems during the evolution of a transcurrent fault system and injection of arc-related, calc-alkaline and hydrous magmas into transtensional gashes or pull-apart domains. The Darreh-Zerreshk and the Ali-Abad granitoid intrusions and associated mineralization, as well as other intrusions in the vicinity, were coeval with the formation of transtensional structures within conjugate shears in the strike-slip DBF system during a period of relaxation of the compressive tectonic regime.

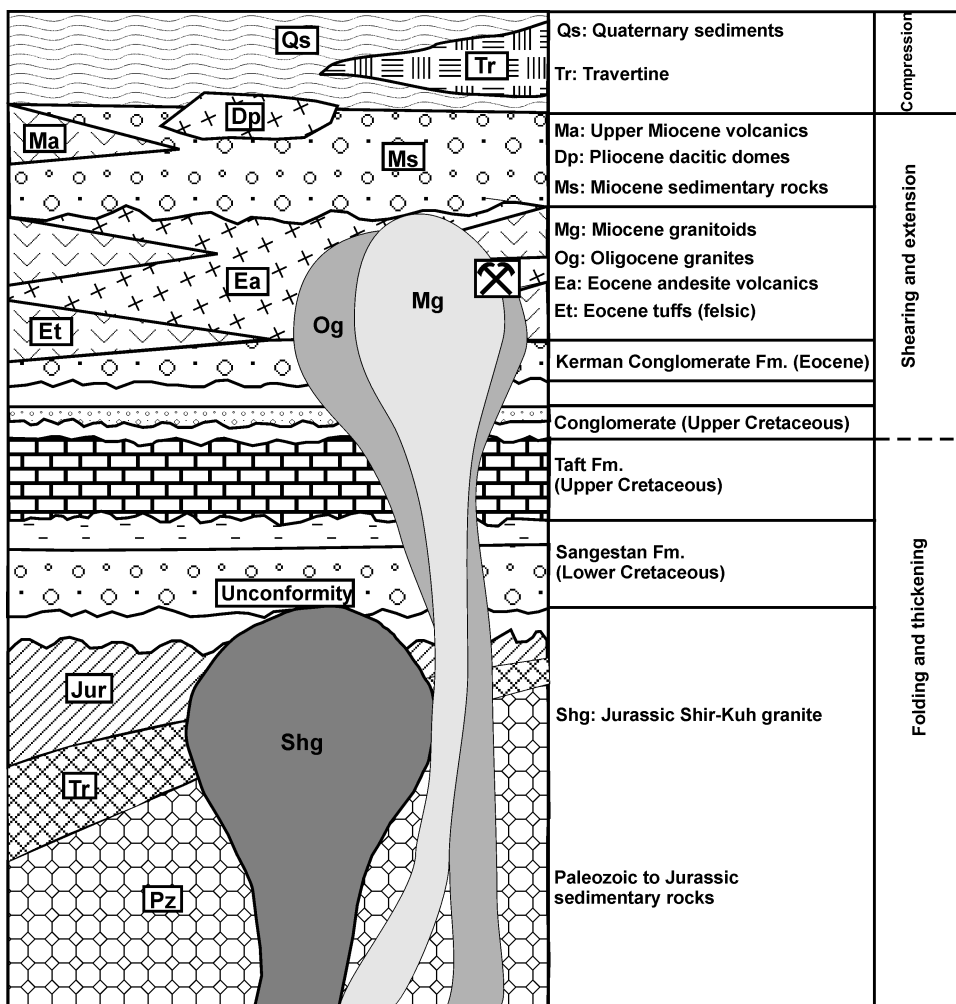


FIG. 15. Summary schematic diagram depicting relative age relationships in the Darreh-Zerreshk and Ali-Abad porphyry copper districts.

Comparison with other deposits in Iran

The alteration, mineralization, geological setting, rock composition, and trace-element composition of the Darreh-Zerreshk and Ali-Abad deposits are similar to those of the better known and large Sungun and Sar-Cheshmeh porphyry copper-molybdenum deposits (e.g., Waterman and Hamilton, 1975; Hezarkhani and Williams-Jones, 1998). Table 3 summarizes general characteristics of major porphyry copper deposits in Iran. Besides tonnage, one of the major differences between Darreh-Zerreshk and Ali-Abad and the larger ones is the lack, or only

a weak development, of a supergene blanket in Darreh-Zerreshk and Ali-Abad. Factors such as insufficient pyrite, unfavorable climate, hydrology, and topography possibly were not conducive to such development, or supergene zones developed earlier were subsequently eroded.

Conclusions

The geological evolution of the Darreh-Zerreshk and Ali-Abad areas can be summarized as follows, illustrated schematically in Figure 15: (1) eruption of pre-mineralization Eocene dacites and andesites

in a compressional tectonic regime; (2) accumulation of clastic and epiclastic sediments in basins and subsequent folding; (3) intrusion of I-type, equigranular granites, followed by exhumation and shallow intrusion of mineralizing Oligo-Miocene porphyry granitoids and development of extensional faults within the Dehshir-Baft strike-slip shear system, immediately followed by porphyry-type alteration and mineralization in granitoid rocks; (4) erosion and exhumation of the porphyry systems; (5) eruption of mafic and felsic volcanics rocks onto the resulting unconformity; (6) a supergene enrichment zone was formed in both deposits, but was possibly removed by erosion in the Darreh-Zerreshk deposit, where a second blanket is presently forming near the water table at ~30 m depth.

The geological, geochemical, and structural investigation of the Darreh-Zerreshk and the Ali-Abad deposits leads to the following conclusions:

1. The Darreh-Zerreshk and the Ali-Abad deposits are true porphyry copper deposits in terms of mineralogy, alteration, structure, and style of magmatism.

2. The deposits occur in a plutonic complex containing dioritic-quartz dioritic, quartz monzodioritic, and more evolved granitic rocks. The granites, however, are relatively older than the intermediate rocks, and are barren. It is the dioritic-quartz dioritic to quartz monzodioritic porphyries that brought in the mineralization.

3. Two different intrusions (Oligocene to Late Miocene) are present in the Darreh-Zerreshk and the Ali-Abad areas. Both have I-type, arc-magmatic geochemical characteristics. These rocks form two mineralized groups; one group evolved under relatively reduced or relatively reduced conditions, and the other under more oxidized conditions that favored the formation of porphyry copper deposits. Thus the mineralized porphyries have abundant magnetite that makes them recognizable in geophysical surveys.

4. Mineralizing igneous rocks were emplaced in transtensional domains structurally related to the evolution of the Dehshir-Baft fault (DBF) shear system.

5. In addition to controlling the emplacement of mineralizing porphyries, the structural study suggests that these were emplaced in an active, strongly anisotropic system, so that transtensional pull-apart basins in strike-slip and en-echelon faults controlled the permeability for porphyry copper-type mineralization. Particularly favorable are fractures

of N-S and NE-SW orientation. Increased pre-ore and syn-ore permeability was important inasmuch as supergene enrichment has been minimal; thus the economic feasibility of these porphyries will depend to a great extent on their hypogene grades.

6. Identification of pull-apart basins and parallel secondary shear zones related to strike-slip faults by ground surveys or remote sensing, as well as the geochemical characterization of granitoids localized within these structures, are useful tools for grass-roots exploration for porphyry copper deposits in the porphyry copper provinces of Iran.

Acknowledgments

The present study constitutes a major component of the first author's Ph.D. thesis at Shiraz University, Iran. The authors thank the National Iranian Copper Industries Company for permission to publish the data and for supplying important unpublished databases. Shiraz University is thanked for funding analyses. The first author thanks the Ministry of Sciences, Research, and Technology of Iran for financial support of his short research stay at Dalhousie University. This work was supported by grants from NICICO and Shiraz University; limited funds were provided by a Discovery grant to M. Zentilli of Dalhousie University from the Natural Sciences and Engineering Research Council of Canada (NSERC). We thank Dr. Jarda Dostal of St. Mary's University, Halifax for his advice on REE geochemistry and Dr. Nick Culshaw of Dalhousie University for criticizing the structural interpretations. Debra Wheeler and Ali Faghie helped in the preparation of illustrations for this manuscript. Valuable reviews by Drs. Nick Badham (UK), Rod Kirkham (Canada), and Victor Maksaev (Chile) significantly improved this manuscript.

REFERENCES

- Alavi, M., 1980, Tectonostratigraphic evolution of the Zagros of Iran: *Geology*, v. 8, p. 144-149.
- Alavi, M., 1994, Tectonics of the Zagros orogenic belt of Iran: New data and interpretations: *Tectonophysics*, v. 229, p. 211-238.
- Amidi, S. M., 1975, Contribution al etude biostratigraphique, petrologique et petrographique des roches magmatiques de la region Natanz-Nain-Surk (Iran Centrl). Unpubl. Ph.D thesis, University of Grenoble, France, 250 p.

- Bazin, D. H., and Hubner, H., 1969, Copper deposits in Iran: Teheran, Iran, Geological Survey of Iran, Report no. 13, 232 p.
- Berberian, F., Muir, I. D., Pankhurst, R. J., and Berberian, M., 1982, Late Cretaceous and Early Miocene Andean-type plutonic activity in northern Makran and central Iran: *Journal of the Geological Society of London*, v. 139, p. 605–614.
- Berberian, M., 1976, Generalized fault map of Iran, 1:5000 000: Teheran, Iran, Geological Survey of Iran.
- Berberian, M., and King G. C. P., 1981, Towards a paleogeography and tectonic evolution of Iran: *Canadian Journal of Earth Sciences*, v. 18, p. 210–265.
- Burnham, C. W., 1979, Magma and hydrothermal fluids, in Barnes, H. L., ed., *Geochemistry of Hydrothermal ore deposits*, 2nd ed: New York, Wiley Interscience, p. 71–136.
- Chappell, B., and White, A. J. R., 1974, Two contrasting granitic types: *Pacific Geology*, v. 2, p. 173–174.
- Chevren, V. B., 1986, Tethys-marginal sedimentary basin in western Iran: *Geological Society of America Bulletin*, v. 97, p. 516–522.
- COFMINS Co., 1972, Geology and feasibility study of the Darreh-Zerreshk and the Ali-Abad deposits: Tehran, Iran, unpubl. report.
- Dehghani, B., 2000, Petrology and geochemistry of magmatism and metamorphism studies in the Darreh-Zerreshk and Touranposht area, southwestern Yazd Province: Unpubl. M.S. thesis, Tehran University, Tehran, Iran, 107 p. (in Persian).
- Dewey, J. F., Pitman, W. C., Ryan, W. B. C., and Bonnin, J., 1973, Plate tectonics and evolution of the Alpine system: *Geological Society of America Bulletin*, v. 84, p. 3137–3180.
- Ellis, R., 1991, Sar-Cheshmeh: *Mining Magazine*, October, p. 192–196.
- Forster, H., 1978, Mesozoic–Cenozoic metallogenesis in Iran: *Journal of the Geological Society of London*, v. 135, p. 443–455.
- Hajmolaali, A., and Alavi, N. M., 1993, Geological map of Khezr-Abad area, scale 1:100,000: Teheran, Iran, Geological Survey of Iran.
- Hanson, G. N., 1980, Rare earth elements in petrogenetic studies of igneous systems: *Annual Review of Earth and Planetary Sciences*, v. 8, p. 371–406.
- Hezarkhani, A., and Williams-Jones, J. A., 1998, Controls of alteration and mineralization in the Sungun porphyry copper deposits, Iran: Evidence from fluid inclusions and stable isotopes: *Economic Geology*, v. 93, p. 651–670.
- Irvine, T. N., and Baragar, W. R. A., 1971, A guide to the chemical classification of the common volcanic rocks: *Canadian Journal of Earth Science*, v. 8, p. 523–548.
- Jankovic, S., 1984, Metallogeny of the Alpine granitoids in the Tethyan-Eurasian metallogenic belt, in *Proceedings of the 27th International Geological Congress*, Moscow, August 4–14, v. 12: Utrecht, Netherlands, VNU Science Press, p. 247–273.
- Khosrotehrani, K., and Vazirimoghadam, H., 1993, Stratigraphy of Lower Cretaceous in south and southwest of Yazd: *Journal of Earth Sciences, Geological Survey of Iran*, no. 7, p. 43–57 (in Persian).
- Lang, J. R., and Titley, S. R., 1998, Isotopic and geochemical characteristics of Laramide magmatic system in Arizona and implication for the genesis of porphyry copper deposits: *Economic Geology*, v. 93, p. 138–170.
- Lindsay, D. D., 1997, Structural control and anisotropy of mineralization within the Chuquicamata porphyry copper deposit, Northern Chile: Unpubl. Ph.D thesis, Dalhousie University, Halifax, Nova Scotia, Canada, 381 p.
- Lowell, J. D., and Guilbert, J. M., 1970, Lateral and vertical alteration mineralization zoning in porphyry ore deposits: *Economic Geology*, v. 65, p. 373–408.
- Maksaev, V., 1990, Metallogeny, geological evolution, and thermochronology of the Chilean Andes between latitudes 21° South, and the origin of major porphyry copper deposits: Unpubl. Ph.D. thesis, Dalhousie University, Halifax, Nova Scotia, Canada, 554 p.
- Merzbacher, C., and Eggler, D. H., 1984, A magmatic geohygrometer application to Mount St. Helens and other dacitic magmas: *Geology*, v. 12, p. 587–590.
- Miyashiro, A., 1977, Nature of alkalic volcanic series: *Contributions to Mineralogy and Petrology*, v. 66, p. 91–110.
- Mohajjel, M., Fergussen, C. L., and Sahandi, M. R., 2003, Cretaceous–Tertiary convergence and continental collision, Sanandaj-Sirjan zone, Western Iran: *Journal of Asian Earth Sciences*, v. 21, p. 397–412.
- Nabavi, M. H., 1972, Geologic map of Yazd quadrangle, scale 1:250,000: Tehran, Iran, Geological Survey of Iran.
- Nabavi, M. H., 1976, An introduction to the geology of Iran, Geological Survey of Iran, 110 p. (in Persian).
- Nakamura, E., 1985, The influence of subduction processes on the geochemistry of Japanese alkaline basalts: *Nature*, v. 316, p. 55–58.
- Nancy, M. T., 1983, Phase equilibria of rock-forming ferromagnesian silicates in granitic systems: *American Journal of Sciences*, v. 283, p. 993–1033.
- Niazi, M., and Asoudeh, I., 1978, The depth of seismicity in the Kermanshah region of Zagros Mountains (Iran): *Earth and Planetary Science Letters*, v. 40, p. 270–274.
- Nicolas, I. A., and Harrison, K. L., 1980, Experimental rare earth element partition coefficients for garnet, clinopyroxene, and amphibole coexisting with andesitic and basaltic liquids: *Geochimica et Cosmochimica Acta*, v. 44, p. 287–308.
- NICICO (National Iranian Copper Industries Co.), 2001, Geology of Ali-Abad area: Tehran, Iran, unpubl. company report (in Persian).

- Richards, J. P., Boyce, A. J., and Pringle, M. S., 2001, Geologic evolution of the Escondida area, northern Chile: A model and temporal localization of porphyry Cu mineralization: *Economic Geology*, v. 96, p. 271–305.
- Riedel, W., 1929, Zur mechanik geologischer Brucherscheinungen: *Centralblatt für Mineralogie, Geologie und Paläontologie, Abhandlung B*, p. 354–368.
- Sabzehei, M., 1974, Les mélanges ophiolitique de la region de Sphandagheh (Iran meridional). Etude petrolique et structurale, interpretation dans le carde Iranian: Unpubl. Ph.D. thesis, University of Grenoble, France, 205 p.
- Sengör, A. M. C., 1990, A new model for the Late Paleozoic–Mesozoic tectonic evolution of Iran and implication for Oman Region: *Geological Society of London Special Publication*, v. 49, p. 797–831.
- Shahabpour, J., 1996, Use of drainage trends as a prospecting tool in the central Iranian porphyry copper belt: *CIM Bulletin*, v. 89, p. 70–75.
- Shahabpour, J., 1999, The role of deep structures in the distribution of some major ore deposits in Iran, NE of Zagros thrust zone: *Journal of Geodynamics*, v. 28, p. 237–250.
- Soffel, H. C., Davoudzadeh, M., Rolf, C., and Schmidt, S., 1996, New paleomagnetic data from Central Iran and a Triassic palaeoreconstruction: *Geologische Rundschau*, v. 85, p. 293–302.
- Sokoutis, D., Bonini, M., Medvedev, S., Boccaletti, M., Talbot, C. J., and Koyi, H., 2000, Indentation of a continent with a built-in thickness change: Experiment and nature: *Tectonophysics*, v. 320, p. 243–270.
- Stocklin, J., 1968, Structural history and tectonics of Iran: A review: *American Association of Petroleum Geologists Bulletin*, v. 52, p. 1229–1258.
- Stocklin, J., 1974, Possible ancient continental margins in Iran, in Burke, K. A. and Drake, C. A., eds., *The geology of continental margins*: New York, NY, Springer, p. 837–887.
- Streckeisen, A., and Lemaitre, R. W. L., 1979, A chemical approximation to modal QAPF classification of the igneous rocks: *Neues Jahrbuch für Mineralogie, Abhandlungen*, v. 136, p. 169–206.
- Sun, S., and McDonough, W. F., 1989, Chemical and isotopic systematics of oceanic basalts: Implications for mantle composition and processes: *Geological Society of London Special Publication*, v. 42, p. 313–345.
- Takin, M., 1972, Iranian geology and continental drift in the Middle East: *Nature*, v. 235, p. 147–150.
- Waterman, G. C., and Hamilton, R. L., 1975, The Sarcheshmeh porphyry copper deposit: *Economic Geology*, v. 70, p. 568–576.
- Woodcock, N. H., and Schubert, C., 1994, Continental strike-slip tectonics, in Hancock, P. L., ed., *Continental deformation*: Oxford, UK, Pergamon Press, p. 251–263.
- Zarasvandi, A., and Liaghat, S., 2003, The role of strike-slip faults in emplacement of Darreh-Zerreshk and Ali-Abad porphyry copper deposits, southwestern Yazd Province, in 7th Geological Society of Iran, Esfahan, Iran, p. 102–112 (in Persian with English abstract).
- Zarasvandi, A., Liaghat, S., and Ghayouri, K., 2002, Geochemical characteristics and tectonic setting of Darreh-Zerreshk and Ali-Abad, southwestern Yazd Province, in 21st Earth Sciences Symposium of Iran: Teheran, Iran, Geological Survey of Iran, p. 481–482 (in Persian with English abstract).
- Zarasvandi, A., Liaghat, S., and Zentilli, M., 2004, Evolution of the Darreh-Zerreshk and Ali-Abad porphyry copper deposits, central Iran, within an orogen-parallel strike-slip system [abs.], in 30th Annual Meeting of Atlantic Geoscience Society, January 30–31, Moncton, New Brunswick, Canada, p. 36.
- Zengqian, H., Hongwen, M., Zaw, K., Yuquan, Z., Mingjie, W., Zeng, W., Guitang, P., and Renli, T., 2003, The Himalayan Yulong porphyry copper belt: Product of large-scale strike-slip faulting in eastern Tibet: *Economic Geology*, v. 98, p. 125–145.